Master Thesis
Jan Grzegorzewski

Reaction-Diffusion Dynamics With Fractional Brownian Motion

Winter term: 2016

Contents

Motivation

Anomalous diffusion can be observed in many different areas of nature, in particular, related to heterogeneous media like porous rocks, gels and crowded biological media with its prominent phenomena macromolecular crowding, confinement and macromolecular adsorption [1]. These environments exhibit remarkable characteristics like anomalous diffusion with its most popular power-law behavior of the mean-square-displacement ($\delta r^2(t) \propto t^\alpha$) [2], which violates the Einstein formula $\delta r^2(t) = 2dDt$ and thereby the central limit theorem. Anomalous diffusion is described by various theoretical models like time random walks (CTRW) with unconventional waiting time-distribution, the Lorentz models with excluded volume and a highly ramified remaining space or fractional Brownian motion (fBm). The latter is modeling a stochastic process with strong correlations of the increments. FBm was first introduced as a family of Gaussian random functions by Mandelbrot and Van Ness in 1968 and motivated by examples in economics [3]. In contrast to different models of anomalous diffusion, the fBm approach is plainly phenomenologically defined by a power-law increase of the MSD and thus perfectly qualifies as a starting point to study effects resulting from a power-law increase of the MSD.

This thesis focuses on the impact of fBm on enzymatic reaction kinetics in three dimension space. Pioneer work by Leonor Michaelis and Maud Menten [4] simplified enzymatic reaction kinetics and formulated a model based on the law of mass action. As one of the best known and important models of enzyme kinetics it is of great interest to study effects on Michaelis-Menten like reactions by fBm. For this purpose a particle based simulation with an fBm integrator of a Michaelis-Menten like reactions was set up. Spatial and temporal effects induced by fBm were studied.

The thesis is organized in four chapters: The first chapter sets up theoretical foundations for fBm. Subsequently, fBm generating algorithms are studied. Chapter 2 deals with models describing reactions in general but focuses on particle-based reaction diffusion. A particle-based Reaction Diffusion software RevReaDDy, which served as a starting point for the implementation is introduced. Chapter 3 focuses more specifically on enzyme reactions. Followed by an enzymatic simulation model set up with RevReaDDy. Finally results from the simulation are discussed and related to existing literature. Chapter 4 summarizes the content of the thesis.

1 Fractional Brownian Motion

The Wiener process is a continuous-time stochastic processes, which models white noise. It is applied to finance, biology, physics and many more if no or only week correlations of the underlying processes are present. Brownian motion is the random motion of particles suspended in a fluid, which is modeled by a wiener process. Velocities of particles however are always correlated at least for very short lag times in the physical world. It is often referred to as the super diffusive regime. Water molecules in water as an example forget there initial velocities in ca. 16Fs. For longer times Brownian motion can be assumed.

Fractional Brownian Motion (fBm) is a more general family of stochastic Gaussian processes then standard Brownian motion with long-range correlations as its defining property. The main objective of this chapter is to explore the theoretical foundation for fBm starting with Brownian motion in the following section. Further algorithms generating fBm are introduced and analyzed in terms of accuracy and performance.

1.1 Brownian Motion

Standard Brownian Motion (Bm) is a very important and well studied stochastic process. It describes the erratic motion of mesoscopic particles, which first were documented by Jan Ingenhousz in 1785, in particular for coal dust on the surface of alcohol [2]. Later on, in 1827 Robert Brown observed the erratic motion of pollen grains. Brownian motion has a Gaussian propagator, which has its origin in the Central Limit Theorem (CLT) for a sum of independent and identically distributed random variables (i.i.d.). Let's assume a set of N independent variables $\{X_j\}$ with a finite variance $\sigma_j^2 = \langle X_j^2 \rangle$ and the mean $\langle X_j \rangle = 0$. The definition of another random variable Y is given by:

$$Y = \frac{1}{\sqrt{N}} \sum_{j=1}^{N} X_j \tag{1.1}$$

This scenario in which a random variable is defined by the sum of another can be observed generically in nature. X_j are called increments of Y. The seemingly innocent assumption of independent increments result in a Gaussian distribution of $\rho(y)$ in the limit of large N with $\rho(y)dy = \mathrm{P}(y < Y < y + dy)$

$$\rho(y) = \frac{1}{\sqrt{2\pi}\sigma} e^{-\frac{y^2}{2\sigma^2}} \tag{1.2}$$

A derivation of this very interesting result can be found in the appendix 5.1. Microscopic processes with i.i.d. velocities, thus have a Gaussian distribution for the overall change in position. Indeed, even the increments of Brownian motion are distributed Gaussian as a result of i.i.d. velocities at shorter time scales. A random walk in the limit of very small time steps therefore converges to Brownian motion.

With Bayes' theorem and an initial delta-distribution one can show that transition probability $T_t(y|0) = \rho_t(y)$ is equivalent to the particle density distribution. One can find the calculation in the appendix section 5.2. The above-mentioned elaborations motivate the reason for a process with a Gaussian transition probability. A processes with Gaussian distributed transition probability and independent increments is called Wiener process (Standard Brownian motion).

Brownian motion described by the Wiener process is a stochastic process $\{W_t\} : \Omega \to \mathbb{R}^d$ with $W_t(\omega)$ being the position of a particle with $\omega \in \Omega$ at time $t \in T$ in the observation time $T = [0, \infty)$. It has a fixed $x \in \mathbb{R}^d$ as its origin. The transition probabilities are [5]:

$$
\begin{aligned}
&T_t(y|x) := (2\pi t)^{-\frac{d}{2}} exp\left(-\frac{||x-y||^2}{2t}\right) \text{ for } y \in \mathbb{R}^d, t > 0 \qquad (1.3)\\
&T_0(y|x) = \delta(x-y)
\end{aligned}
$$

The Wiener process is a Gaussian process with mean $\langle W_t \rangle_y = x$ and particle position $W_o = x$ at $t = 0$. Its variance is $\langle W_t^2 \rangle_y = t$. It has stationary, independent, Gaussian increments. Following from the definition Brownian motion has the property called Brownian scaling:

$$
\{\hat{W}_t := \frac{1}{c} W_{c^2 t}\}_{t \geq 0} \qquad (1.4)
$$

A Wiener process has self-similar and fractal paths as a result from Brownian scaling.

However it is a purely mathematical model with missing connection to the strength of diffusion of a particle. The process in fact is a normalized diffusion process with the a diffusion constant $D = \frac{1}{2}$. A mathematical description of diffusion was first realized by Fick in 1855 [6]. He applied partial differential equations for heat transfer first solved by Fourier in 1822 [7]. Fick's second law of diffusion describes how diffusion causes the concentration $(c(\boldsymbol{r}, t))$ to change over time:

$$
\frac{\partial}{\partial t} c(\boldsymbol{r}, t) = -\nabla J(\boldsymbol{r}, t) = D \Delta c(\boldsymbol{r}, t) \qquad \text{with} \qquad \Delta = \nabla^2 \qquad (1.5)
$$

With Fick's first law $J(\boldsymbol{r}, t) = -\nabla c(\boldsymbol{r}, t)$ and D being the flux of particles and the diffusion coefficient, respectively. The notation of bold letters is chosen to describe vectors (e.g. $\boldsymbol{r}$). Fick's first law is a result from the linear response theory. Fick's second law can be derived from mass conservation and Fick's first law. The most general form of mass conversation with a production term σ is described by the continuity equation:

$$\frac{\partial}{\partial t}c(\boldsymbol{r},t)) = -\nabla J(\boldsymbol{r},t) + \sigma \tag{1.6}$$

Albert Einstein in 1905 proposed a similar equation to Fick's second law of diffusion to solve one dimensional Brownian motion [8]. This was the first derivation and application of probabilistic stochastic theory. Derived from the kinetic gas theory and a statistical description collisions in 1906 Marian von Smoluchowski could give similar results to Einstein [9]. The concentration $c(\boldsymbol{r},t)$ is proportional to the transition probability $\mathrm{P}(\boldsymbol{r},t) \propto c(\boldsymbol{r},t)$ and $\int d\boldsymbol{r}\mathrm{P}(\boldsymbol{r},t) = 1$. The transition probability of the Wiener process builds the foundation for a more physical description of particle motion by a propagator:

$$\mathrm{P}(r,t) = (4\pi Dt)^{-\frac{d}{2}} \exp\left(-\frac{r^2}{4Dt}\right) \tag{1.7}$$

The propagator $\mathrm{P}(r,t)$ can be interpreted as the probability to move the distance r during the time t. d is the dimension of the space of $\boldsymbol{r}$. One can show that this propagator is in fact solving the diffusion equation eq. (1.5) with the meaningful initial condition of vanishing concentration at boundaries:

$$c(\pm\infty,t) = 0 \tag{1.8}$$

The calculation can be found in the appendix 5.3. The most important property of Brownian motion in the context of this thesis is the mean square displacement ($\delta r^2(t)$), which grows linearly with the number of steps:

$$\delta r^2(t) =< [\boldsymbol{R}(t) - \boldsymbol{R}(0)]^2 >= 2dDt \tag{1.9}$$

with $\boldsymbol{R}(t)$ being the position of the particle at time t. Brownian scaling was mentioned as a property of a Wiener process. It obviously also applies as a property to the propagator of Brownian motion. A scale-free form of the Gaussian propagator exists as a more intuitive consequence of Brownian scaling:

$$\mathrm{P}(r,t) = r^{-d}\mathcal{P}_{gauss}(\hat{r}) \tag{1.10}$$

$$\text{with} \quad \hat{r} = \frac{r}{\sqrt{2Dt}} \quad \text{and} \quad \mathcal{P}_{gauss}(\hat{r}) = (2\pi)^{-\frac{d}{2}}\hat{r}^d \exp\left(-\frac{\hat{r}^2}{2}\right) \tag{1.11}$$

The scale free form of Bm can later on be compared to the scale free form of fractional Brownian motion, which will be introduced next. This property results in a neat possibility of analysis of Bm and fBm generating algorithms later on.

1.2 Fractional Brownian Motion

In the previous section the MSD has been shown to be linear with time as a result of the central limit theorem. In normal liquids this behavior can be seen already at

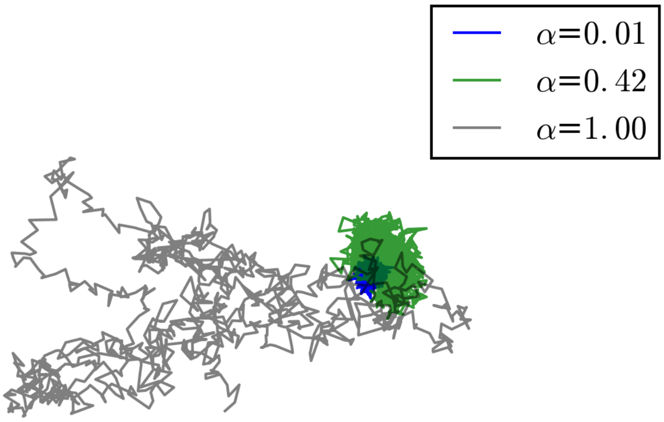

Figure 1.1: A three dimensional fBm trajectories for the anomalous coefficient $0.01 \leq \alpha \leq 1$ generated with the Lowen algorithm are shown. The general diffusion constant, the time step and trajectory length were chosen as follows: $K_\alpha = 1$, $\Delta t = 1$, $M = 1000$.

time scales higher than picoseconds [2]. Nevertheless, many experiments show that the MSD has a power law behavior ($\delta r^2(t) \propto t^\alpha$ for $0 < \alpha < 1$) over certain time windows form microseconds to even seconds. Thus, the central limit theorem does not hold, at least in theses time scales. It can be shown that persistent correlations of the increments are present. In soft matter, like polymers, a sub-diffusive behavior is typically present in a time window but finally the linear MSD takes over. Fractional Brownian motion idealizes this situation by imposing that the central limit theorem is violated even for all time scales. The basic feature of fBm's is that the "span of interdependence" between their increments can be said to be infinite [3]

Just like the Wiener process, continuous-time Fractional Brownian motion (ctfBm) is a continuous-time Gaussian process $\{B_t^\alpha\} : \Omega \to \mathbb{R}^d$ at time $t \in T$ in the observation time $T = [0, \infty)$. It is fully specified by its mean $\langle B_t \rangle = 0$ and its covariance function:

$$\mathrm{Cov}[B_t^\alpha, B_s^\alpha] = \frac{\sigma^2}{2}[t^\alpha - 2(s-t)^\alpha + s^\alpha] \qquad \text{for} \qquad t < s \tag{1.12}$$

With the mean and the covariance defined, the mean square displacement for fBm can be derived as:

$$\langle (B_t^\alpha - B_s^\alpha)^2 \rangle = (s-t)^\alpha \sigma^2 \tag{1.13}$$

Fractional Brownian motion exhibits a power law behavior of the mean square displacement and therefore indeed motivates to act as a model for anomalous diffusion.

Fractional Brownian motion can be alternatively expressed in terms of its incremental sequence. The incremental sequence is a related stochastic process called continuous-time fractional Gaussian noise (ctfGn). CtfGn is a continuous-time

Gaussian process $\{X_t^\alpha\} : \Omega \to \mathbb{R}^d$ at time $t \in T$ in the observation time $T = [0, \infty)$. The mean is zero $\langle X_t^\alpha \rangle = 0$ and variance $\mathrm{Var}[X_t^\alpha] = \langle (X_t^\alpha)^2 \rangle = \sigma^2$:

$$B_t^\alpha = \int_s^t X_{t'}^\alpha dt' + B_s^\alpha \qquad \text{for} \qquad t < s \tag{1.14}$$

The covariance function for ctfGn can be derived from the covariance function of fractional Brownian noise:

$$\begin{aligned} \mathrm{Cov}[X_t^\alpha, X_s^\alpha] &= \frac{d^2}{dtds} \mathrm{Cov}[B_t^\alpha B_s^\alpha] = -\sigma^2 \frac{d^2 |t-s|^\alpha}{dtds} && (1.15) \\ &= \alpha(\alpha - 1)\sigma^2 |t-s|^{\alpha-2} + \alpha\sigma^2 |t-s|^{\alpha-1} \delta(t-s) && (1.16) \end{aligned}$$

The first term of this covariance function is describing the correlation of the increments. For Wiener white noise ($\alpha = 1$) the first terms disappears:

$$\mathrm{Cov}[X_t, X_s] = \sigma^2 \delta(t-s) \tag{1.17}$$

The description of fractional Brownian motion in terms of fractional Gaussian noise is often convenient because of fGn's stationarity. The spectral density function can be written due to the Wiener-Khintchin theorem as the Fourier transform of the auto-covariance function:

$$S(\omega) = \int_{-\infty}^{\infty} \mathrm{Cov}[X_t, X_0] \exp[-2\pi i \omega t] dt \tag{1.18}$$

For algorithmic purpose discrete time fractional Brownian motion (fBm) and Gaussian noise (fGn) are relevant as well:

$$B_t^\alpha = \sum_{i=0}^{k} X_i^\alpha \tag{1.19}$$

The covariance function for fBm is similar to ctfBm but different for fGn in comparison to ctfGn:

$$\begin{aligned} \mathrm{Cov}[X_n^\alpha, X_m^\alpha] &= \langle (B_n^\alpha - B_{n-1}^\alpha)(B_m^\alpha - B_{m-1}^\alpha) \rangle \\ &= \frac{\sigma^2}{2} [(n-m-1)^\alpha - 2(n-m)^\alpha + (n-m+1)^\alpha] \\ \text{for} \quad n \geq m \end{aligned}$$

and with stationarity:

$$\mathrm{Cov}[X_0^\alpha, X_m^\alpha] = \frac{\sigma^2}{2} [(n-1)^\alpha - 2n^\alpha + (n+1)^\alpha] \tag{1.20}$$

A more detailed study on fBm and fGm can be found in [10]. Similar to the argumentation for Brownian motion also fBm need a connection to the strength of diffusion. This connection is introduced by the variance of fGn as:

$$\sigma^2 = 2dK_\alpha \Delta t \tag{1.21}$$

The Mean square displacement for fBm follows from eq. (1.13) as:

$$\delta r^2(t) =< \Delta R(t)^2 >= 2dK_\alpha t^\alpha \tag{1.22}$$

with $K_\alpha > 0$ being the generalized diffusion coefficient. It is not quite the diffusion constant from Fick's law due to different units.

In the following properties of a more physical description of fBm will be discussed:

- The single particle density $\rho(\boldsymbol{r}, t) = \delta(\boldsymbol{r} - \boldsymbol{R}(t))$ describes the density of a particle, which is localized at position $\boldsymbol{R}(t)$. Its correlation function $P(\boldsymbol{r} - \boldsymbol{r}', t - t') = V\langle\rho(\boldsymbol{r}, t)\rho(\boldsymbol{r}', t')\rangle$ is also called Van Hove self-correlation function (in this context the propagator). V refers to the volume. From now on we will consider an isotropic system $r = |\boldsymbol{r}|$. As for Brownian motion with independent increments the correlated increments $\Delta R(t)$ of fractional Brownian motion are assumed to follow a Gaussian distribution with zero mean. Thus the correlation function of the single particle density results in:

$$P(r, t) = [2\pi\delta r^2(t)/d]^{-\frac{d}{2}} e^{\frac{-r^2 d}{2\delta r^2(t)}} \tag{1.23}$$

- The propagator of fBm can be transformed into a scale free form. It is related to the scale free from of standard Brownian motion eq. (1.11):

$$P(\boldsymbol{r}, t) = \boldsymbol{r}^{-d}\mathcal{P}_{gauss}(\hat{\boldsymbol{r}}) \qquad \text{with} \qquad \hat{\boldsymbol{r}} = \frac{\boldsymbol{r}}{\sqrt{2K_\alpha t^\alpha}} \tag{1.24}$$

- The van hove correlation function can be transformed via the spatial Fourier transform into its wave-number representation, which is called the self-intermediate scattering function. Again for isotropic systems one can write $|\boldsymbol{k}| = k$.

$$F_s(k, t) = \langle\rho(k, t)\rho(k', t')\rangle = \int d^d r e^{-ikr} P(r, t) \tag{1.25}$$

$$= \langle e^{-ik\Delta R(t)}\rangle \tag{1.26}$$

- The intermediate scattering function for the single particle density turns out to be the characteristic or moment generating function of $\Delta R(t)$ by expanding it for small wave numbers $k \to 0$ one can get the moments. Its logarithm returns the cumulants. For Gaussian propagators with zero-mean all but the second cumulants vanish. For non-Gaussian transport also further cumulants are non-zero. Therefore, it is used to indicate beyond Gaussian transport. The non-Gaussian parameter is defined as:

$$\alpha_2 = \frac{d\delta r^4(t)}{(d+2)[\delta r^2(t)]} - 1 \tag{1.27}$$

- An other important quantity is the dynamical structure factor, which is the time-frequency Fourier transform of the intermediate scattering function:

$$F_s(k,z) = \langle \rho(k,z)\rho(k',z')\rangle = \int_0^\infty dte^{-itz}P(k,t) \text{ for } k \to 0, \mathrm{Im}(z) > 0 \tag{1.28}$$

$$= \frac{1}{-iz} - \frac{k^2}{2d}\int_0^\infty dte^{izt}\delta r^2(t) + \mathcal{O}(k^2) \tag{1.29}$$

For the velocities as our random variables $\partial_t \boldsymbol{R}(t) = \boldsymbol{\xi}(t)$ also the Velocity auto correlation function is of interest. Velocities correspond to continuous-time fractional Gaussian noise in the mathematical description.

- Velocities can be used to calculated the Velocity Autocorrelation Function (VACF):

$$Z(|t-t'|) = \frac{1}{d}\langle \boldsymbol{\xi}(t)\boldsymbol{\xi}(t')\rangle = \frac{1}{2d}\frac{d^2}{dt^2}\delta r^2(t-t') \tag{1.30}$$

The VACF in the frequency domain for fBm is:

$$\tilde{Z}(z) \overset{\mathrm{Im}(z)>0}{=} K_\alpha \Gamma(1+\alpha)(iz)^{1-\alpha} \tag{1.31}$$

The calculation can be found in the appendix 5.4

1.3 Algorithm

The algorithm of choice will be needed as the integrator of motion in a particle based reaction-diffusion software with preferably long trajectories. Therefore exactness and performance of the algorithm matter. In literature several algorithms were studied. Promising exact methods are: Cholesky [11], Hosking [12], Davis-Harte [11] and Lowen [13] method. Cholesky method claim to perform $\mathcal{O}(M^3)$ in respect to the length of trajectory M and even $\mathcal{O}(M^2)$ for every next trajectory. Davis-Harte and Lowen method claim to be exact and fast $\mathcal{O}(Mlog(M))$ [14][13]. There are further algorithms with even faster performance (e.g. the $RMD_{3,3}$- method [11] with $\mathcal{O}(M)$) . However, they are approximations. In order to choose an algorithm. Three algorithms were analyzed in terms of accuracy and speed. 1.Cholesky 2.Lowen and 3. Our own algorithm.

Cholesky Method

(cite the thesis of Ton Dieker) $\mathcal{O}(M^3)$

Our Algorithms

The VACF in the frequency domain will be used to modify standard Brownian motion velocities, which are easily computable, to generate increments. The starting point are the velocities $\partial_t \boldsymbol{R}(t) = \boldsymbol{\xi}(t)$. The increments can be decomposed in its Fourier modes for real frequencies $z = \omega$:

$$\tilde{\boldsymbol{\xi}}_T(\omega) = \int_{-\frac{T}{2}}^{\frac{T}{2}} dt e^{i\omega t} \boldsymbol{\xi}(t) \tag{1.32}$$

For a finite observation time T the Wiener-Khinchin theorem applies :

$$\lim_{T\to\infty} \frac{1}{T} \langle |\tilde{\boldsymbol{\xi}}_T(\omega)|^2 \rangle = 2\,\mathrm{Re}\left(\tilde{Z}(\omega)\right) \tag{1.33}$$

For white noise one gets:

$$\lim_{T\to\infty} \frac{1}{T} \langle |\tilde{\boldsymbol{\eta}}_T(\omega)|^2 \rangle = const. \tag{1.34}$$

Fractional correlations can be incorporated via its VACF:

$$\tilde{\boldsymbol{\xi}}(\omega) = \sqrt{2\,\mathrm{Re}\left(Z\tilde{(\omega)}\right)}\tilde{\boldsymbol{\eta}}(\omega) \tag{1.35}$$

With $\tilde{\boldsymbol{\xi}}(\omega)$ being fractional Brownian velocities in the frequency domain. Its Fourier-back-transform results in fractional Brownian velocities in the time domain.

$$\boldsymbol{\xi}(t) = \int d\omega e^{i\omega t} \tilde{\boldsymbol{\xi}}(\omega) \tag{1.36}$$

In the following an algorithm, which generates fractional Brownian noise will be introduced. The algorithm is based on the Davis-Harte algorithm [15]. The idea is to use the calculated VACF and thereby modify conventionally generated Gaussian random variables. All the increments should be generated beforehand. With this concept it is difficult to include forces. For computational reasons the previous elaborations on how to generate fractional Brownian increments have to be transformed into a discrete form, thereby the solution is no longer exact, which will be shown in the analysis part of the algorithm.

$$\boldsymbol{\eta}(t) \longrightarrow \boldsymbol{\eta}_j(t) \text{ with } j = 0, 1, 2, ..., n \ , \ n = \text{amount of steps} \tag{1.37}$$

For a n-steps long trajectory one can write:

$$\Delta \boldsymbol{R}_n(t) = \sum_{j=0}^{n} \boldsymbol{\eta}_j \Delta t \tag{1.38}$$

The following algorithm is explained for one dimension and can be easily extended for more dimensions. The MSD can be written as:

$$< \Delta R_j(t) >= 2K_\alpha(\Delta tj)^\alpha \tag{1.39}$$

The algorithm goes as follows:

1. M independent normally distributed random increments are generated:

$$\eta_k(t) = \mathcal{N}(0, \sqrt{\Delta t}) \text{ with } k = 0, 1, 2, ..., M \tag{1.40}$$

   $M > n$ more increments are generated to counteract the boundary problem in the discrete Fourier transform, which is shown in fig. 1.2(a) and fig. 1.2(b)

2. Via discrete Fourier transform these increments are transformed into the frequency domain:

$$\tilde{\eta}_l(z) = \sum_{k=0}^{M-1} \eta_k e^{\frac{-i2\pi lk}{M}} \Delta t \text{ with } l = 0, 1, 2, ..., M \tag{1.41}$$

$$\tag{1.42}$$

   By comparison with the eq. (1.32) one can see that:

$$z \to l\Delta z \text{ , } \Delta z = \frac{2\pi}{M\Delta t} \text{ , } t \to j\Delta t \text{ and } \int dt \to \sum \Delta t \tag{1.43}$$

3. Comparable to eq. (1.35) correlations are incorporated:

$$\tilde{\xi}_l(z) = \tilde{\eta}_l(z)\sqrt{2Re(\tilde{Z}_l(z))} \tag{1.44}$$

   with $\tilde{Z}(z) \to \tilde{Z}_l(z)$ as introduced in eq. (1.43):

$$\tilde{Z}_l(z) = K_\alpha\Gamma(1+\alpha)(i2\pi l\Delta z)^{1-\alpha} = K_\alpha\Gamma(1+\alpha)(il\frac{2\pi}{M\Delta t})^{1-\alpha} \tag{1.45}$$

4. The discrete Fourier transform has a downside compared to the continuous Fourier transform, as already noted in the beginning of this section. The VACF is zero at zero-frequency $\tilde{Z}_{l=0}(z = 0) = 0$. From eq. (1.44) also the first increment in the frequency domain is zero $\tilde{\xi}_{l=o}(z = 0) = 0$. Due to eq. (1.41) also the following relation holds:

$$\tilde{\xi}_{l=o}(z) = \sum_{k=0}^{M-1} \xi_k e^0 \Delta t = \Delta R_M \tag{1.46}$$

   ΔR is the distance between the starting point and the position of the particle. Therefore, the particle would travel after M steps back to its initial position.

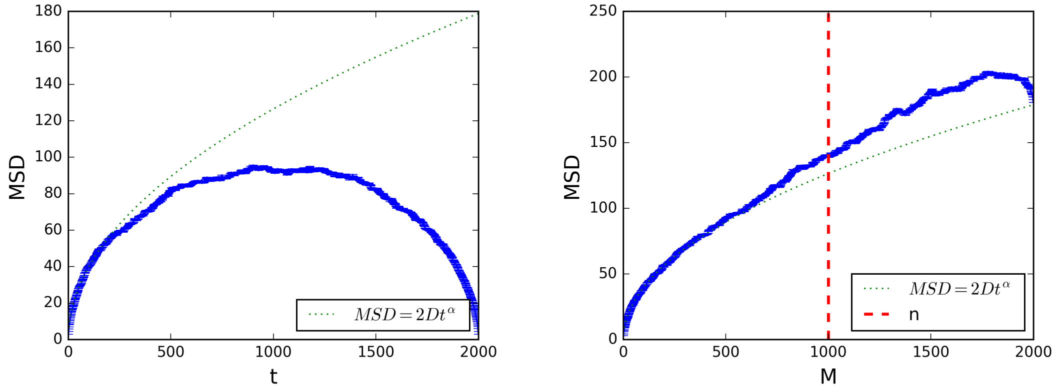

(a) Ensemble MSD without the correction introduced in eq. (1.46)

(b) Ensemble MSD with correction introduced in eq. (1.46). The side of the red bar indicates the threshold for the remaining increments for $M = 2n$

The effect on the ensemble averaged mean square displacement can be seen in fig. 1.2(a). Instead, the zero-increment in the frequency domain is calculated as follows:

$$\tilde{\xi}_{l=o}(z) = \mathcal{N}(0, \sqrt{2K_{\alpha}(M\Delta t)^{\alpha}}) \tag{1.47}$$

This equation would be correct if we assumed fractional Brownian motion to be a Markovian process, which certainly is not the cause. This is also the reason why M have been chosen to be bigger than n. The presumption is, that the impact of the approximation would be negligible with increasing distance to ΔR_M and negligible at ΔR_n. The impact on the ensemble averaged MSD can be seen in fig. 1.2(b). This can be thought of as a finite-time correction.

5. Fractional Brownian increments in the time domain result from the reverse Fourier transform:

$$\xi_k = \frac{1}{2n} \sum_{l=0}^{2n-1} \tilde{\xi}_l e^{\frac{2\pi i l k}{2n}} \Delta z \tag{1.48}$$

Only n increments are taken into account ξ_j for $j = (0, 1, .., n)$.

The described algorithm can be performed independently for every Cartesian component of the three dimensional fractional Brownian motion. The Cartesian component are not correlated.

Lowen

The previous algorithm had down draws in terms of convergence close to 0 and close to the overall simulation time. therefore a algorithm of Steven B. Lowen [13] had been implemented. Lowens algorithm claims to be both both fast ($\mathcal{O}(NlogN)$) and exact. However our implementation show not to be exact, which can be seen in the analysis part. The algorithm goes as follows:

1. Compute a periodic auto-covariance function of $R_\xi(n)$ of a stochastic process $\xi(n)$:

$$R_\xi(n) = \begin{cases} \frac{1}{2}\left[1 - \left(\frac{n}{N}\right)^\alpha\right] & \text{for } 0 \leq n \leq N \\ R_\xi(2N-n) & \text{for } N \leq n \leq 2N \end{cases} \tag{1.49}$$

2. Transform the auto-covariance function via FFT. The result is called the spectral density of the stochastic process $\xi(n)$:

$$S_\xi(k) = FFT(R_\xi(n)) \tag{1.50}$$

3. Calculate $\tilde{\xi}(k)$ the Fourier transform of the stochastic process $\xi(n)$:

$$\tilde{\xi}(k) = \begin{cases} 0 & \text{for } k = 0 \\ exp(i\theta)\eta\sqrt{S_\xi(k)} & \text{for } 0 \leq k \leq N \\ \eta\sqrt{S_\xi(k)} & \text{for } k = N \\ \tilde{\xi}^*(2N-k) & \text{for } N \leq k \leq 2N \end{cases} \tag{1.51}$$

$\tilde{\xi}^*$ denotes the complex conjugate of $\tilde{\xi}$. θ is a random variable uniformly distributed in $(0, 2\pi]$. η is a random Gaussian variable with zero mean and variance 1 ($\mathcal{N}(0,1)$).

4. Perform the inverse Fourier transform on $\tilde{\xi}(k)$ and use the first half of the resulting stochastic process $\xi(n)$ multiplied by a factor:

$$\xi(n) = FFT^{-1}(\tilde{\xi}(k)) \tag{1.52}$$

$$B_n^\alpha = \sqrt{2K_\alpha N^\alpha \Delta t^\alpha}(\xi(n) - \xi(0)) \qquad \text{for } 0 \leq n \leq N \tag{1.53}$$

Lets check the resulting auto-covariance function.

$$Cov[B_n^\alpha, B_m^\alpha] = 2K_\alpha \Delta t^\alpha N^\alpha \langle(\xi(n) - \xi(0))((\xi(m) - \xi(0))\rangle \tag{1.54}$$

$$= 2K_\alpha \Delta t^\alpha N^\alpha \langle \xi(n)\xi(m)\rangle - \langle \xi(0)\xi(m)\rangle - \langle \xi(0)\xi(n)\rangle + \langle \xi(0)^2\rangle \tag{1.55}$$

$$= \frac{2K_\alpha \Delta t^\alpha}{2}[n^\alpha - 2(m-n)^\alpha + n^\alpha] \qquad \text{for } n < m \tag{1.56}$$

The auto-covariance function indeed satisfies the condition for fBm with variance similar to eq. (1.21). In step 3 the phase and amplitude of the Fourier transform $\xi(m)$ were chosen to be random as suggested in [16]. The second derivative of $R_\xi(n)$ is positive. $R_\xi(n)$ results in a periodic function with non negative curvature. Its Fourier transform $S_\xi(k)$ is , real, symmetric and non-negative for all k. $S_\xi(k)$ is then a valid power spectral density function of the discrete-time periodic process $\xi(n)$

with period $2n$ and $R_\xi(n)$ its valid auto-covariance function [13]. This algorithm is actually using the property of Brownian scaling eq. (1.4) to generate a realization of fBm with non negative auto-covariance function. The algorithm was implemented in c++ with a 1 dimension Fast Fourier transform from the package FFTW3. FFTW computes an unnormalized DFT. Thus, computing a forward followed by a backward transform results in the original array scaled by the size of the array. The size of the array is $2M$ in Lowens algorithm. Thus a random variable should be divided by $\sqrt{2N}$ to have a normalized FFT.

Accuracy Analysis

The algorithms were implemented in python and c++. For the c++ implementation a wrapper to python was added. All algorithms have been analyzed by an analysis class. The c++ implementation is using FFTW library for the Fast Fourier Transform and Mersenne-Twister (gsl_rng_mt19937) as the random number generator. Python implementations were developed beforehand and only serve as reference. Python uses the numpy.fft library for the Fast Fourier Transform and also the Mersenne-Twister random number generator.

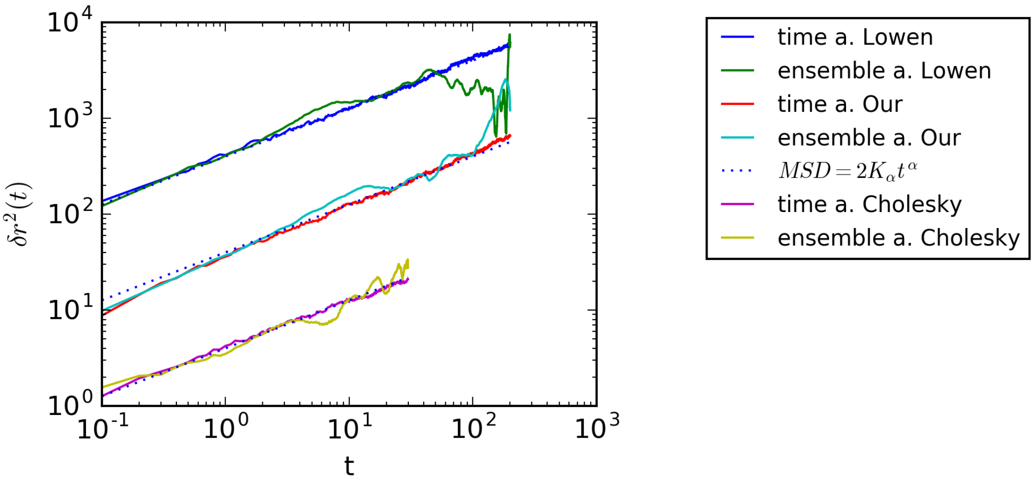

Figure 1.2: Comparison of MSD between time-average, ensemble-average ($N = 1000$) ,$\alpha = 0.5$, $\Delta t = 0.1$ for the three algorithms.
Cholesky: $D = 2$, $M = 300$.
Our $D = 20$ $M = 2000$,
Lowen: $D = 200$ $M = 2000$.

To get insight into stochastic algorithms observables have to by studied. Observables of an stochastic process are generally averaged values. The motivation of choosing fBm was its power law behavior of the MSD. It is therefore to be reasonable to analyze first this observable. It can be calculated as the ensemble- or time average. A difference in time and ensemble average would show a violation of ergodicity. A comparison for all the three implemented algorithms can be seen in fig. 1.2. All algorithm show good accuracy between ensemble and time averaged MSD, besides for long lag times for the time averaged MSD due to decreasing statistics. Our algorithm tend to result in too small MSDs for small lag times particularly for small α, which is going be shown later on. This is caused by the finite amount of samples in the discrete Fourier transform. In the following figures all MSD plots are ensemble averages. They are computationally cheaper.

Secondly time-reversibility had been checked. FBm should be time reversible as shown in [17]. In fig. 1.3 MSDs for forward time and for backward time were plotted. No difference can be seen. α had been chosen to be 0.1. Thereby our algorithm has an even stronger deviation from the desired power law. A strong influence of α on

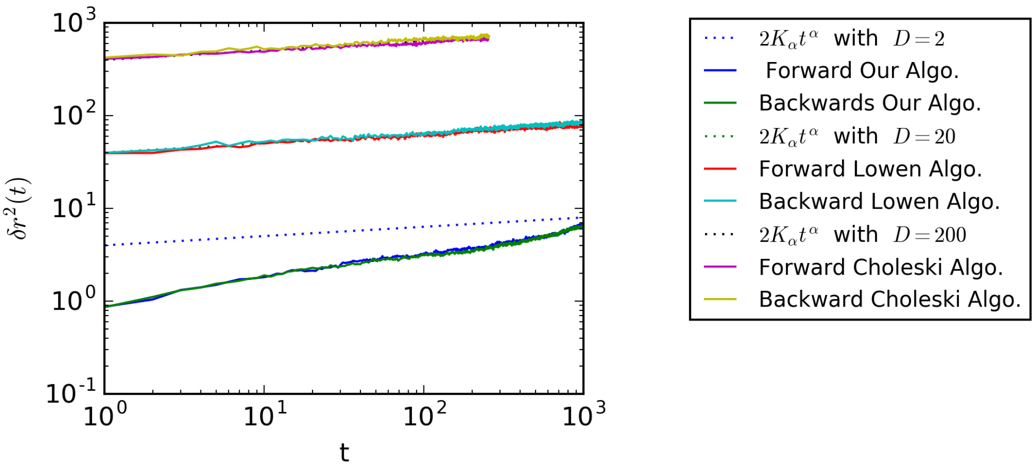

Figure 1.3: The plot show ensemble averaged MSDs for forward time and backward time over $N = 2000$ trajectories for $\alpha = 0.1$, $\Delta t = 0.1$ and trajectory length $M = 1000$ and $K_\alpha = 2$ for Our algorithm, $M = 1000$ $K_\alpha = 20$ for Lowen algorithm and $M = 256$ $K_\alpha = 200$ for Cholesky algorithm.

the accuracy of MSD for our algorithm can be seen. The influence of α on the MSD for the three algorithms are shown in fig. 1.4. In the limit of Brownian motion $\alpha = 1$ the artifacts for small lag-times in the our algorithm vanish. Cholesky and Lowen show no deviation to the expected MSD for all α.

FBms property of self similarity can be used to plot a scale free version of the density distribution. The scale free version was introduced in eq. (1.24). The scaled density distribution is not depended on time but overlaps for all times. In fig. 1.5 histograms over $N = 10000$ single trajectories at various times ($100 \leq t \leq 1000$) were calculated and rescaled according to eq. (1.24). The dashed line show the expected distribution. For Cholesky and our algorithm no deviations from the analytical line is obvious. For Lowens algorithm systematically small changes to the analytical value can be observed. However, the distribution of fBm should stay a Gaussian for all times. As introduced in eq. (1.27) the non-Gaussian parameter should be zero. The Non-Gaussian parameter has been plotted for $0 \leq t \leq 1000(\leq 356$ for Cholesky) $\alpha = 0.5$ in fig. 1.6 a). Our and Cholesky algorithm perform as expected. Lowen

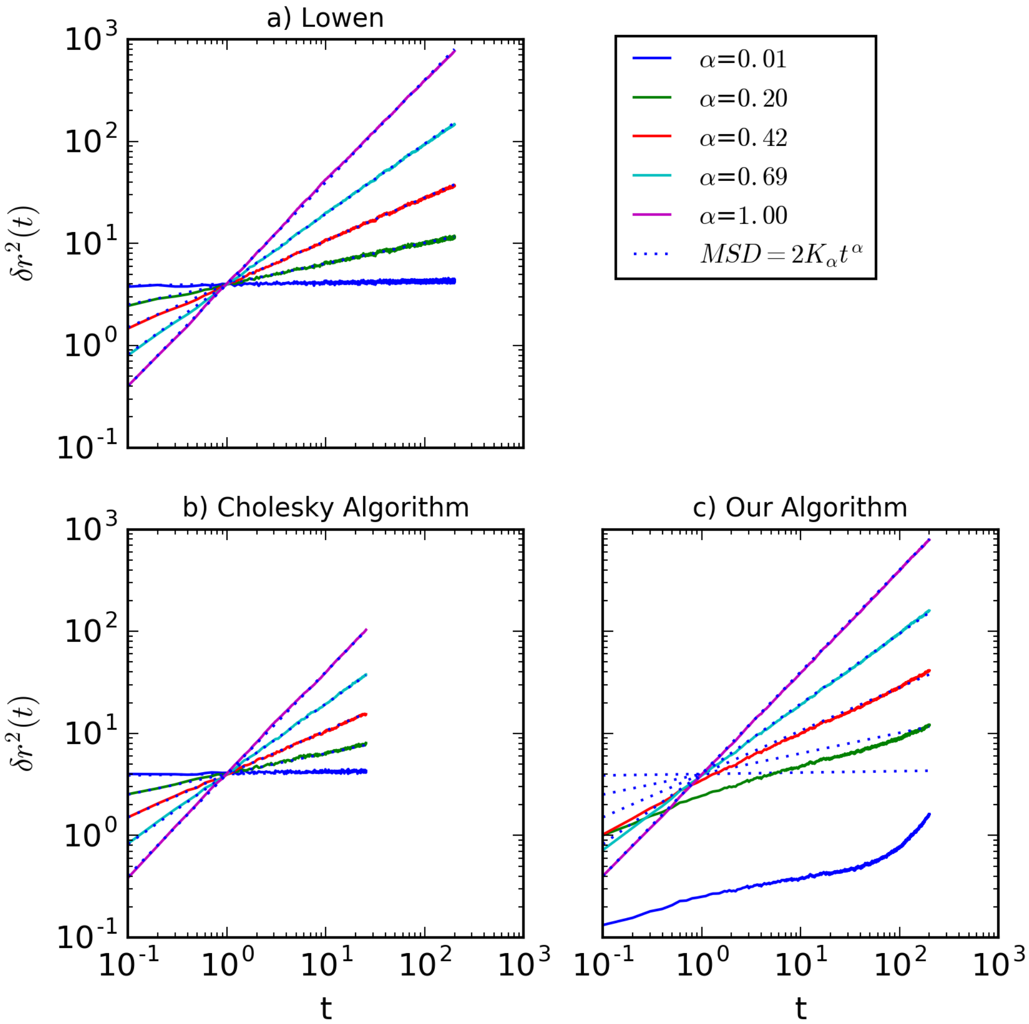

Figure 1.4: All three plots show an ensemble averaged MSD over $N = 2000$ trajectories for $0.1 < \alpha < 1.0$ with $K_\alpha = 2$,$\Delta t = 0.1$ and trajectory length $M = 2000$ for Our and Lowen algorithm, $M = 256$ for Cholesky algorithm. a) Our algorithm and b) Lowen algorithm c) Cholesky algorithm.

however show deviation from a Gaussian distribution increasingly towards the end of the trajectory. In fig. 1.6 b) the influence of α on the non-Gaussian parameter for the Lowen algorithm was tested. For small α the distribution is closer to a Gaussian. In our implementation Lowens algorithm is not exact as claimed in [13].

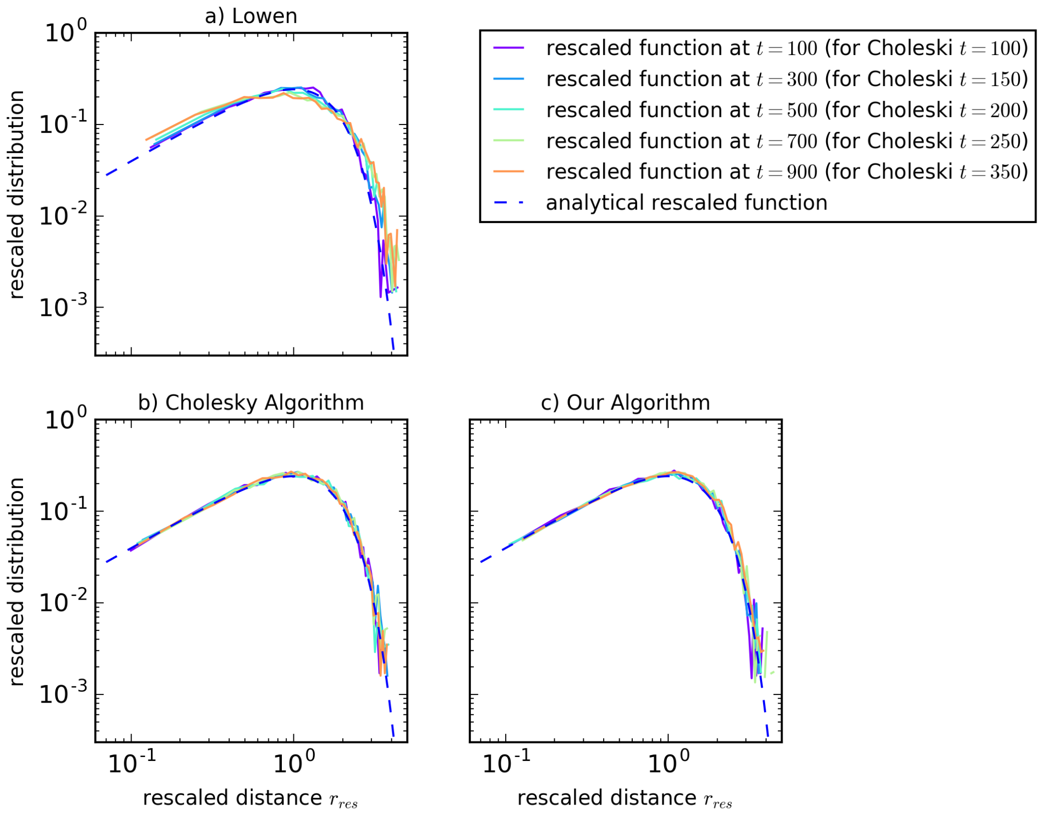

Figure 1.5: All three plots show the scale free form of the propagator at different times as introduced in eq. (1.24) as an histogram over $N = 10000$ trajectories for $\alpha = 0.5$ with $K_\alpha = 2$,$\Delta t = 0.1$ for all three algorithm, at different times $100 < t < 900$

Performance Analysis

The performance in respected to sample size (trajectory length) and number of samples (amount of trajectories) was analyzed in fig. 1.7 b) . Thereby the most promising, in terms of exactness, Cholesky algorithm scales in respect to the trajectory length M with $\mathcal{O}(M^3)$. Our application of the integrator desire long trajectories. It is not reasonable to use such a slow algorithm. Even if every next trajectory with the same α and length is of $\mathcal{O}(M^2)$ [11]. In fig. 1.7 a) one can see Cholesky to scale slow with the amount of trajectories N. Although one should keep in mind that the trajectory length had to be chosen $M = 128$ compared to $M = 1000$ as for Our and Lowens algorithm to get comparably small values. Lowens and Our algorithm perform both $\mathcal{O}(Mlog(M))$ in respect to the trajectory length as a result of the FFT and $\mathcal{O}(N)$ in respect to the amount of trajectories.

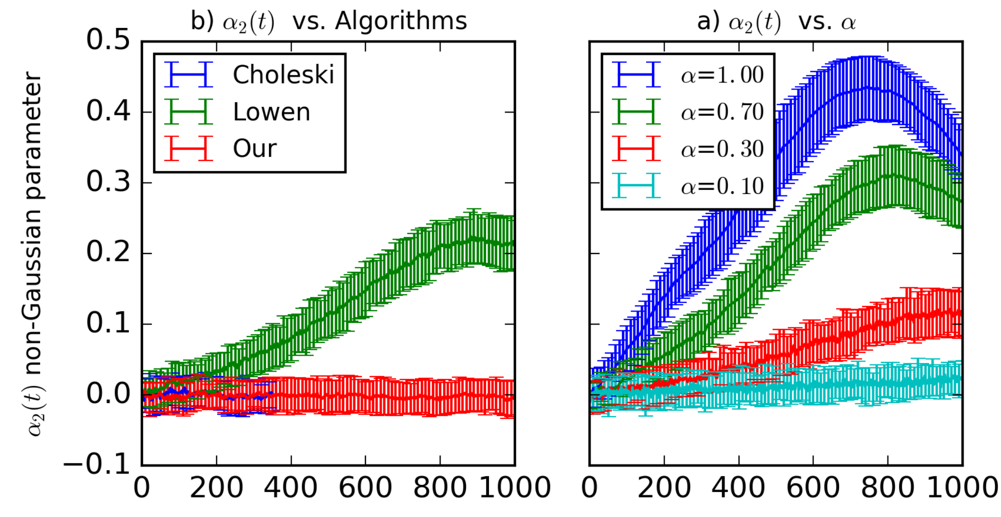

Figure 1.6: a) Non-Gaussian-Parameter as introduced in eq. (1.27) for all three algorithms with $K_\alpha = 2$, $N = 5000$,$\alpha = 0.5$ (Lowen and Our $M = 1001$; Cholesky $M = 356$), $\Delta t = 1$ averaged over 50 non-Gaussian-Parameter with its variance displayed as an error bar.
b) Non-Gaussian-Parameter for Lowen algorithms with $K_\alpha = 2$, $N = 5000$, $M = 1001$, $\Delta t = 1$ and for various $0.1 \leq \alpha \leq 1.0$ averaged over 50 non-Gaussian-Parameter with its variance displayed as an error bar.

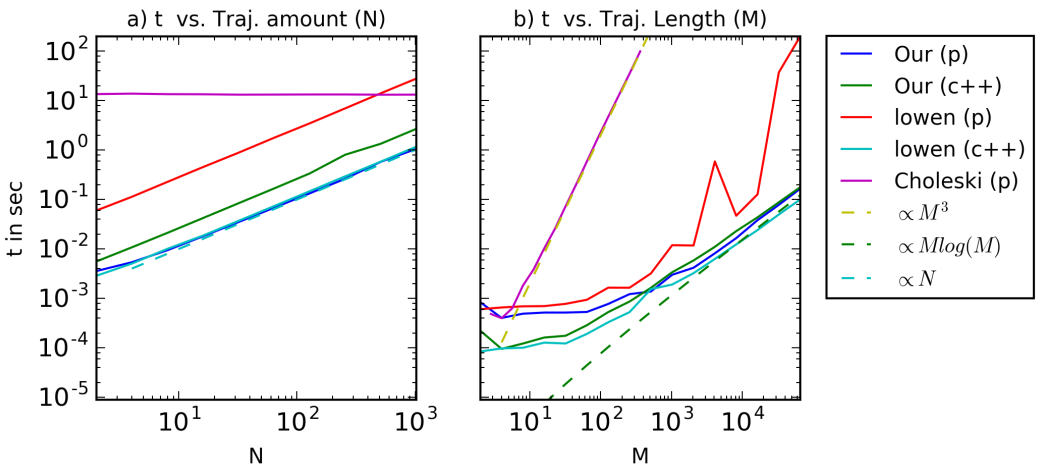

Figure 1.7: a) Algorithmic scaling of computational time in respect to the amount of trajectories N for trajectory length $M = 1000$, ($D = 2$, $\alpha = 0.5$, $\Delta t = 1$) of Lowen and our own algorithm. Both implemented in c++ and python (p). The Cholesky algorithm was implemented in python with $M = 128$.
b) Algorithmic scaling of computational time in respect to the trajectory length M for a single trajectory $N = 1$, ($D = 2$, $\alpha = 0.5$, $\Delta t = 1$). Lowen and our own algorithms are implemented in c++ and python (p). Cholesky is only implemented in python (p).

2 Particle Based Reaction Diffusion

Chemical reactions are generically found in nature. They describe a transformation of chemical substances to one another, transformations of chemical substances are described by formation and breaking of chemical bonds. These bonds are formed due to electromagnetic forces. Physically correct theses bonds should be described quantum mechanically. For large systems these calculation cannot be performed, so coarse grained models for the description were developed. But reactions in a broader sense can also be a transformations of a state to another (e.g. protein changing its transformation). The most detailed standard model is given by particle-based reaction-diffusion dynamcis (PBRD). Thereby all particles are modeled as points or spheres and are resolved in space and time. However, the size particularly of common biological systems surpass computational feasibility. So further coarse graining gets necessary. Early pioneer work on reactions by Guldberg and Waage already in 1864 [18] resulted in the law of mass action, which states the proportionality of the reaction rate to the concentration for elementary molecular reactions. Thereby spatial resolution is neglected. The system is described in terms of a concentration (well-mixed assumption). The mass action law leads to a deterministic model described by ordinary differential equations (ODEs). Quantities like reaction kinetics and amount of reactants in equilibrium can be obtained. Deterministic models however are not resolving stochastic phenomena. Stochastic models provide a more detailed understanding of the reaction-diffusion processes. Such a description is often necessary for the modeling of biological systems where small molecular abundances of some chemical species make deterministic models inaccurate or even inapplicable [19]. Stochastic models based on the mass action law are characterized by the chemical Master equation (CME). CME describes the temporal evolution of the probabilities for the system to occupy each different state. The interesting topic of chemical kinetics described by CME will not be part of the elaborations. Nevertheless, for the sake of completeness, it was to be mentioned that stochastic simulations based on CME with the Gillispie algorithm [20] are performing very efficiently. Even spatial resolutions can be achieved with simulations based on the reaction-diffusion Master equation (RDME). Still the well-mixed assumption has to hold at least for the compartments of the RDME model. Difficulties in simulation of biological systems arise on the one hand from very large systems and on the other from small molecular abundances of some chemical species. The well-mixed assumption does not hold. A Less prominent approach is a PBRD model with fractional Brownian dynamics. Fractional Brownian motion describes the motion of a particle in crowded biological media. The motion of the media itself has not to be modeled explicitly. Therefore PBRD simulations can be performed just for the relevant reacting particles. Stochastic particle based models conventionally rely on Brownian or Langevin dynamics for the description of diffusion. Brownian dynamics was introduced in chapter 1. Langevin dynamics will not be examined explicitly. In short, it is further considering momentum and reaches Brownian dynamics in the limit of vanishing momentum.

This chapter deals with some theoretical considerations on the impact of diffusion on reaction rates. The first section examines Smoluchwoski pioneer work [21] on diffusion limited reaction kinetics of a bi-molecular reaction and Erban/Chapmman extensions [22] for diffusion influenced bi-molecular reactions. Thereby a dependence of macroscopic reaction rates and the diffusion of the particles can be seen. These results shell motivate investigations of reaction diffusion dynamics with a different diffusion model. Along the way the law of mass action is shown to follow under certain conditions from the diffusion eq. (1.5) motivated and introduced in the first chapter. These derivations further motivate both, concentration and PBRD models. RevReaDDy, a realization of the latter, is then introduced and explained in the second section of this chapter.

2.1 Diffusion Influenced Bimolecular Reaction

Uni- and bi-molecular elementary reactions are most relevant in nature. According to collision theory tre-molecular elementary reactions are negligible. Diffusion is not relevant for uni-molecular reactions. It is reasonable to start our considerations on how diffusion influences chemical reactions with the Smoluchowski problem for kinetics of a bi-molecular chemical reaction in solution. One particular area of research on which the Smoluchowski relation had significant impact in the last few decades is biology. This is unsurprising as a vast number of biomolecular systems involve dilute and minute diffusing molecular populations undergoing continuous reaction. Understanding how these biological systems operate is complicated and is in itself a whole field of research; systems biology. The Smoluchowski result has provided a very powerful tool for theoretical investigation of microscopic biochemical reaction-diffusion processes [23]. It was extended by P. Debye in 1942 to add intermolecular forces. However, especially in biological systems Brownian motion do not apply for all time-scales. These environments exhibit very often anomalous diffusion, which can be addressed by fBm.

The following derivation shell give the kinetics of an easy model for a bi-molecular reaction and motivate a particle based simulation scheme.

The reaction scheme for a bi-molecular reaction with reactants A and B undergo fusion to a complex AB with a rate k_d^+ and undergo fission to A and B with a rate k_d^-. The chemical reaction can be written as:

$$\mathrm{A} + \mathrm{B} \underset{k_\mathrm{d}^-}{\overset{k_\mathrm{d}^+}{\rightleftharpoons}} \mathrm{AB}$$

Free diffusion of particle A and B with the diffusion constants D_A and D_B, respectively, are assumed. Further no interactions between them are present. In fact this problem can be described by a modified version of the diffusion eq. (1.5) motivated in the first chapter. The joint concentration field for a bi-molecular system in a solution can be written as:

$$\frac{\partial \rho_t(\boldsymbol{r}_A, \boldsymbol{r}_B)}{\partial t} = (D_A \nabla_A^2 + D_B \nabla_B^2) \rho_t(\boldsymbol{r}_A, \boldsymbol{r}_B) \tag{2.1}$$

The complexity of the problem can be reduced by substituting the positions of the particles A and B with their relative distance $\boldsymbol{r} = \boldsymbol{r}_A - \boldsymbol{r}_B$. It is convenient to introduce even further substitutions:

$$D = D_A + D_B \qquad \boldsymbol{R} = \frac{D_B \boldsymbol{r}_A + D_A \boldsymbol{r}_B}{D_A + D_B} \tag{2.2}$$

the Laplace operator in terms of new coordinates result in:

$$\nabla_A^2 = \left(\nabla_r + \frac{D_B}{D} \nabla_R \right)^2 \tag{2.3}$$

$$\nabla_B^2 = \left(\nabla_r + \frac{D_A}{D} \nabla_R \right)^2 \tag{2.4}$$

By inserting eq. (2.3) and (2.4) in eq. (2.1) the following result can be obtained:

$$\frac{\partial \tilde{\rho}_t(\boldsymbol{r}, \boldsymbol{R})}{\partial t} = \left(D \nabla_r^2 + \frac{D_B D_A}{D_A + D_B} \nabla_R^2 \right) \tilde{\rho}_t(\boldsymbol{r}, \boldsymbol{R}) \tag{2.5}$$

This equation describes two independent diffusion processes, one in the coordinate $\boldsymbol{r}$ and one in the coordinate $\boldsymbol{R}$. The solution can be obtained by the product ansatz $\tilde{\rho}_t(\boldsymbol{r}, \boldsymbol{R}) = \rho_t(\boldsymbol{r}) q_t(\boldsymbol{R})$. Integration over $\boldsymbol{R}$ results in:

$$\frac{\partial \rho_t(\boldsymbol{r})}{\partial t} = D \nabla_r^2 \rho_t(\boldsymbol{r}) + \frac{D_B D_A}{D_A + D_B} \nabla_R^2 \rho_t(\boldsymbol{r}) \int_{\partial V} q_t(\boldsymbol{R}) d\boldsymbol{a} \tag{2.6}$$

In the previous equation the stokes theorem was applied. The second term is zero due to conservation of probability. The problem is isotropic, hence $r = |\boldsymbol{r}|$ and $\nabla_{\boldsymbol{r}}^2 = \left(\partial_r + \frac{2}{r} \right) \partial$. The equation reduce to one dimension:

$$\frac{\partial \rho_t(r)}{\partial t} = - \left(\frac{\partial}{\partial_r} + \frac{2}{r} \right) j_t(r) \qquad j_t(r) = D \frac{\partial \rho_t(r)}{\partial_r} \tag{2.7}$$

The stationary distribution results in:

$$-\left(\frac{\partial}{\partial_r}+\frac{2}{r}\right)j^s(r)=0 \tag{2.8}$$

$$\frac{dj^s(r)}{j^s(r)}=-\frac{2}{r}dr \tag{2.9}$$

$$j^s(r)=Ar^{-2} \tag{2.10}$$

$$\rho^s(r)=\rho^s(r_0)-\frac{\int_\sigma^r j^s(r')dr'}{D}=\rho^s(r_0)+\frac{A}{D}\left(\frac{1}{r}-\frac{1}{\sigma}\right) \tag{2.11}$$

Now lets assume only a single molecule B being at the position $r=0$. Instantaneous reactions occur for $r\leq\sigma\Rightarrow\rho_t(r\leq\sigma)=0$. For $r\to\infty$ the distribution is defined as the concentration of particle A $\rho_t(r\to\infty)=c_A$. The solutions for $\rho^s(r)$ and $j^s_t(r)$ for theses boundary conditions can be written as:

$$\rho^s(r)=C_A\left(1-\frac{\sigma}{r}\right) \qquad j^s(r)=-D\sigma C_A r^{-2} \tag{2.12}$$

The change of the concentration of C_{AB} is then:

$$\frac{dC_{AB}}{dt}=4\pi\sigma DC_AC_B \tag{2.13}$$

Along the way several assumptions were made:

- The system can be described by a diffusion constant which is independent of time and position.
- No interaction between particles are present (ideal gas).
- The System has a constant concentration of A particles at boundary $\rho_t(r\to\infty)=c_A$.
- The system System is in a stationary distribution.
- The system of one B particle with a concentration $C_B=1/V$ can generalized for a system with many particles.
- The system is in the diffusion limit.

Still the solution gives the kinetics for a simple bi-molecular system. It is consistent with collision theory, which states that the collision frequency is proportional to the concentrations of the colliding particles. Pioneer work on reaction kinetics by Guldberg and Waage already in 1864 [18] resulted in the law of mass action, which states the proportionality of the reaction rate (r_f) to the concentration for elementary uni- and bi-molecular reactions.

$$r_f=k_fC_AC_B \tag{2.14}$$

It builds up the basis for a description of reaction kinetics in terms of ordinary differential equations (ODEs) like eq. (2.13).

Smoluchowski's problem can be in fact generalized for reactions to occur with a microscopic rate λ_+ within a radius σ, derived by R. Erban and S. J. Chapman in [22]. However, as a small remark, the microscopic rate has to be distinguished from the macroscopic rate. As an example microscopic rates are related to the Kramers problem, describing the time dependence of a particle passing a potential barrier e. g. commonly in biology protein binding / unbinding. The generalized problem can be described similarly to Smoluchwoski's problem eq. (2.7) with a similar boundary condition for $r > \sigma$ but different for $r \leq \sigma$:

$$r \leq \sigma \Rightarrow \frac{\partial \rho_t(r \leq \sigma)}{\partial t} = -\lambda_+ \rho_t(r \leq \sigma) \tag{2.15}$$

The derivation of the solution of the second-order ODEs can be found in the Appendix 5.5. The solution shows again the possibility of describing the overall change of concentration with a macroscopic reaction rate $k_+(\lambda_+, \sigma, D)$:

$$k_+ = 4\pi D \left(\sigma - \sqrt{\frac{D}{\lambda_+}} \tanh \sigma \sqrt{\frac{\lambda_+}{D}} \right) \tag{2.16}$$

Reaction kinetics can be described by the law of mass action not only in the diffusion limit but also for reactions occurring with a certain microscopic rate. Under the well mixed assumption and normal diffusion it is possible to formulate ODEs for the system. There solutions give the kinetics and concentrations in equilibrium, but no informations on the spatial distribution are contained.

For the generalized problem with a microscopic rate λ_+ a diffusion and microscopic reaction limit can be shown. For $\lambda_+ \to \infty$ reaction occur immediately and the diffusion limit is reached. If $\lambda_+ \ll \frac{D}{\sigma^2}$ a Taylor expansion of the Tangens Hyperbolicus in eq. (2.16) can be written as:

$$\tanh \sigma \sqrt{\frac{D}{\lambda_+}} \approx \sigma \sqrt{\frac{D}{\lambda_+}} - \frac{\left(\sigma \sqrt{\frac{D}{\lambda_+}} \right)^3}{3} \tag{2.17}$$

and eq. (2.16) can be written approximately as:

$$k_+ = \frac{4\pi\sigma^3\lambda_+}{3} \tag{2.18}$$

The macroscopic reaction rate no longer depends on the diffusion but solely on the microscopic reaction rate. The stationary distributions for both limits and an intermediate scenario are plotted in fig. 2.1.

The previous elaborations show that macroscopic reaction rates dependent on diffusion for bi-molecular reactions. For easy reaction diffusion systems the evolution and the stationary distribution of the density distribution can be obtained by solving Smoluchwoski's equation (PDE). For the bi-molecular reaction the law of

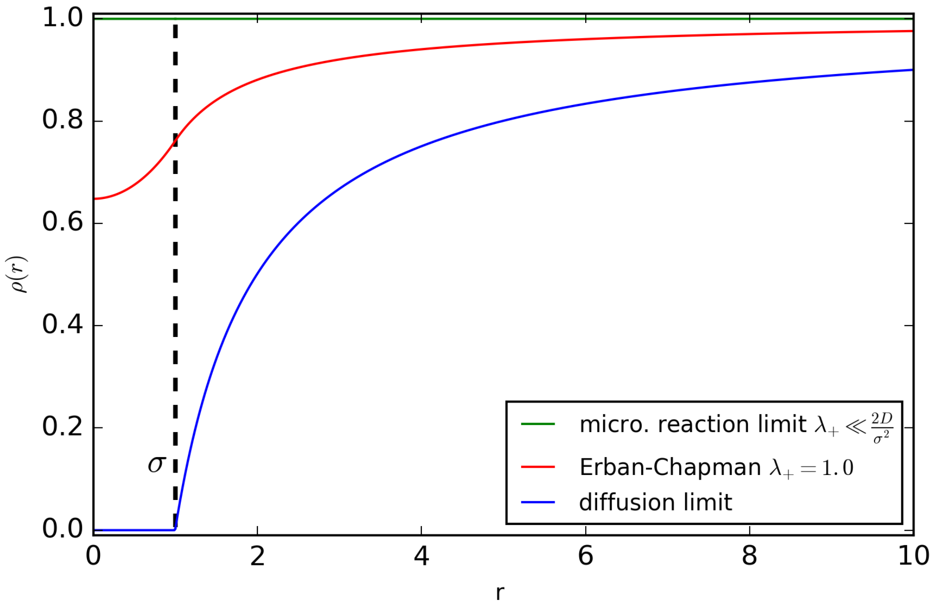

Figure 2.1: Density distribution of three scenarios. 1 reaction limit for $\lambda_+ = 0.0001 \ll \frac{D}{\sigma^2}$, 2. Erban Chapmann with $\lambda_+ = 1$ and 3. In all Diffusion limit with $\lambda_+ \to \infty$. For all scenarios D, σ and $\rho_t(r \to \infty) = c_A$ have been set to 1.

mass action could be seen to follow for spatial homogeneity. Then reaction kinetics can be described for easy systems in terms of ODEs. Nevertheless complex systems cannot be solved. Further, for small molecular abundances of some chemical species deterministic models get inaccurate or even inapplicable. Stochastic models are necessary. Via Chemical Master equations (CMEs) and reaction diffusion Master equations (RDMEs) analytical stochastic results can be obtained. Deduced from the Master equation also stochastic simulations based on Monte Carlo methods, like the prominent Gillispie algorithm [20], can be performed. This chapter however aims to introduce PBRD. The implementation of a PBRD simulation introduced in the next section follows the theoretical description of reactions with microscopic reaction rates within a reaction radius in this section.

2.2 RevReaddy with fBm

RevreaDDy is a PBRD tool developed by Christoph Fröhner. It is not going to be published or further improved. Many modification to the tool had to be done in the process of this thesis. RevreaDDy is based on the simulation package ReaDDy by Johannes Schöneberg and Frank Noé [24]. Reaction-diffusion dynamics of all particles can be resolved in space and time. Particles are modeled as spheres with possible particle interaction potentials. The tool aims to bridge the gap between

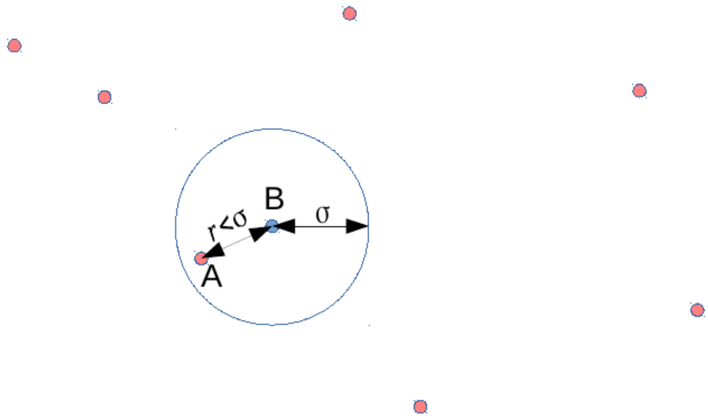

Figure 2.2: The Figure shows a visualization of a bi-molecular reaction between particle A and B in RevReaDDy.

molecular simulation and CME/RDME simulations. It is written in C++. However, the user can setup up and simulate the desired reaction scheme in Python via a Python binding. Particle types with a specific radius and diffusion constant can be defined. Particles of a predefined particle type can be placed anywhere into a simulation box with variable box size and periodic boundary conditions. A desired simulation length and width of the time step have to be set. Conventionally particles propagate by Brownian Dynamics. In the process of the thesis also a fractional Brownian motion integrator with the circulant method by Davis-Harte [11] and Lowen [13] was implement. For Brownian Dynamics potentials with two different potential types, Lennard Jones and soft repulsion, can be introduced to act in-between participles and between fixed geometries in the simulation box and particles. Thereby a temperature has to by defined. Particles can be e.g limited to diffuse on a surface by a potential. It can be chosen from various reaction types to effect the particle types. For Uni-molecular reactions like conversion A $\underset{k'}{\overset{k}{\rightleftarrows}}$ B, decay A $\xrightarrow{k}$ $\emptyset$, fission $A \xrightarrow{k} B + C$ the probability that one particle undergoes a reaction can be given as:

$$P = \lambda \Delta t \tag{2.19}$$

Microscopic reaction rates for a single particle to undergo a reaction λ are independent of the relative position.

For fission a weighting factor and reaction distance can be defined. They determine how far each of the particles are placed from the previously existing complex. For bi-molecular reactions like the enzymatic reaction with complex building $A + B \underset{k'}{\overset{k}{\rightleftarrows}} A + C$ or fusion $A + B \xrightarrow{k}$ C relative positions of the reactants are important for the reaction to take place. Analogous to the setup up of Erban and Chapman in section 2.1 a microscopic reaction rate λ within a reaction distance σ have to be defined. If the reactants come closer than σ a reaction takes place with probability $P = \lambda\Delta t$. The problem is visualized in fig. 2.2. Thereby the time step cannot by chosen arbitrary large. The mean square displacement for Brownian motion in three dimensions is given as $\delta r^2(\Delta t) = 6D\Delta t$. The mean displacement has to be a lot smaller than the reaction distance. Otherwise differences between the time of particles staying within a radius σ to another particle would differ significantly in comparison to $\Delta t \to 0$. Thus also the macroscopic reaction rates would become less accurate. For fractional Brownian motion with $\alpha < 1$ the effect gets even worse. A variety of observables are provided in RevReaddy, which are written into HDF5 files during the simulation. Possible observables are: Acceptance rate, energy, mean square displacement, particle number, radial distribution functions, amount of reactions, increments and positions. Observables can mostly be defined to consider any particle type over any period in time.

3 An Enzymatic Reaction With Fractional Brownian Motion

Enzymes are large biological molecules mostly proteins. They have a key role especially in metabolic processes in cells. They help to break down large nutrient molecules like carbohydrates, fats and proteins during in the process of digestion. Other enzymes contrariwise help forming large and complex molecules from smaller once. Enzymes are involved in storage and release of energy, processes of respiration, vision, muscle contraction, transmission of nerve impulses. In fact biochemical reactions are controlled mainly by enzymes. In general they act as catalysts by lowering the activation energy. As stated by the Arrhenius law the activation energy is then increasing the reaction rates. The speed of reactions is typically increased by $10^6 - 10^{14}$. So reactions with enzymes involved take place a lot faster than without. Enzymes do not change the equilibrium concentrations. Enzymes are mostly proteins. They have a defined amino acid sequence and a three-dimensional structure. The specific three-dimensional structure contains an active side for a substrate molecule to bind and orient and a catalytic site to reduce the chemical activation energy. Usually, an enzyme molecule has only one active site, and the active site fits with one specific type of substrate. So enzymes mostly have a high specificity for a particular type of reaction. Catalysis follows the binding of the substrate to the binding side. Some residues can be both, part of the binding side and catalytic site. The catalytic site lowers the activation energy for the reaction. After reaction takes place the product is released. The enzyme is free to start the reaction with a new substrate. From a single enzyme and single substrate to a single enzyme and single product many reversible intermediate states can be present in the reaction mechanism. A simple representation of the mechanism with two complex intermediate states can be written as:

$$\mathrm{S} + \mathrm{E} \underset{k'_1}{\overset{k_1}{\rightleftharpoons}} \mathrm{ES} \underset{k'_2}{\overset{k_2}{\rightleftharpoons}} \mathrm{EP} \underset{k'_3}{\overset{k_3}{\rightleftharpoons}} \mathrm{P} + \mathrm{E} \tag{3.1}$$

k are the forward rates and k' the backward rates. S and P are substrates and products, respectively. ES and EP are intermediate complexes. By the law of mass action ODEs can be formulated but not solved.

The focus of this chapter is to study the kinetics and spatial distribution of the Michaelis-Menten mechanism, an even simpler mechanism, without and with fractional Brownian motion. Some related theoretical work on the fractional reaction diffusion equation of the Michaelis-Menten mechanism had been done by Abdullah [25]. Monte Carlo simulations with the anomalous diffusion modeled by a random walk and immobile obstacles were performed by Berry and Schnell [26, 27]. An overview on stochastic modeling of in vivo reactions was given by Turner [28]. Recently first passage time simulations with fBm were performed by Jae-Hyung Jeon, A. V. Chechkin and Ralf Metzler [29]. Nevertheless, a Michaelis Menten mechanism with fractional Brownian motion was not yet studied.

3.1 Michaelis-Menten (MM) kinetics

Leonor Michaelis and Maud Menten proposed in 1913 a mathematical model for enzyme kinetics. Their most important contribution was to assume an enzyme-substrate to be present [4]. In their honor it is also called Michaelis-Menten complex. A simpler version of eq. (3.1) was proposed as the Michaelis-Menten mechanism:

$$\mathrm{S} + \mathrm{E} \underset{k_-}{\overset{k_+}{\rightleftharpoons}} \mathrm{ES} \xrightarrow{k_c} \mathrm{P} + \mathrm{E} \tag{3.2}$$

The rate of the backward reaction from products and enzymes to complexes was assumed to be negligible. They postulated the relation between the reaction velocity, formation of products, and the concentration of substrates. This relation is captured by the so called Michaelis-Menten equation:

$$v = \frac{v_{max} c_s}{K_M + c_s} \tag{3.3}$$

v_{max} is the maximum reaction velocity. The Michaelis constant K_M is the substrate concentration with 50% of maximum velocity and c_s is the concentration of the substrate. A derivation of the Michaelis-Menten equation was done by Briggs and Haldane in 1925 assuming the mass action law, mass conservation and a quasi-steady state approximation (QSSA). It states that after a negligible initial transition period ($t > t_c$) the concentration of the complex vary slowly as if in a quasi-steady state $dC_{ES}/dt = 0$. The approximation was shown to hold for $c_{E_0} \ll K_M$ or $K_M \ll c_{S_0}$ [30]. A derivation of eq. (3.3) can be found in the Appendix 5.6. In 1997 a closed form for the kinetics of the Michaelis-Menten mechanism with the quasi-steady state approximation was derived by Schnell amd C.Mendoza [31]:

$$c_S(t) = K_M \mathrm{W}\left(\frac{c_{S_0}}{K_M} \exp\left(\frac{-v_{max} t + c_{S_0}}{K_M}\right)\right) \tag{3.4}$$

$$c_{ES}(t) = \frac{c_{E_0} c_S(t)}{K_M + c_S(t)} (1 - \exp(-(K_M + c_S(t) k_+)) \tag{3.5}$$

$$c_E(t) = c_{E_0}(t) - c_{ES}(t) \tag{3.6}$$

$$c_P(t) = c_{S_0} - c_S(t) + c_{ES}(t) \tag{3.7}$$

$v_{max} = k_2 c_{E_0}$ is the maximum velocity, W(x) is the omega function and the Michaelis-Menten constant is defined as:

$$K_M = \frac{k_- + k_c}{k_+} \tag{3.8}$$

The quasi-steady state approximation was applied in the derivation of $c_S(t)$. A time independent c_{ES} is conventionally solved for the transitions period $t < t_c$ by approximating $c_S(t < t_c) \approx c_{S_0}$. For eq. (3.5) the result for the time independent c_{ES} during the transitions period ($t < t_c$) was extended to the total period of time ($0 < t < \infty$) by applying time depended $c_S(t)$ from eq. (3.4). For normal diffusion theses equation will be used to fit the concentrations resulting from the simulation. Still for a small number of particles deterministic approach may differ from the averages of the stochastic simulation [28].

The quasi equilibrium approximation is the second very common approximation typically applied on setups with high enzyme concentrations. It is assumed that the binding step quickly reaches an equilibrium state ($c_S c_E / c_{ES} = K_S$). $K_S = k_- / k_+$ is the dissociation constant and the rate of product formation can be written as:

$$v = \frac{V_{max} c_S}{K_S + c_S} \tag{3.9}$$

The assumption was shown to be true for $c_{E_0} \gg K_M$ or $k_- \gg k_c$. [30].

A description of the Michaelis Menten mechansim with fractional Brownian motion by fractional fractional diffusion reaction equation [32] was done by Abdullah [25]. An earlier description of reaction kinetics with fractional diffusion was done by Kopelman [33] for a percolation cluster with a scaling theory and an upgraded time depended reaction rates. This concepts were applied by Berry [26] and Schnell [27] for the Michaelis Menten mechanism.

3.2 Simulation Model

The simulation of the Michaelis-Menten mechanism eq. (3.2) and fractional Brownian motion with the circulant method by Davis-Harte [11] was setup up with RevReaDDy. Four particle types were defined: substrate, product complex and enzyme. Substrates and products were set to diffuse with the general diffusion constant $K_\alpha = 1/6$. Enzymes and complexes are modeled to be immobile with $K_\alpha = 0$. Enzymes are often even 100 times heavier than substrates or products and therefore diffuse a lot slower. A single enzyme was set in the origin $(x, y) = (0, 0)$ and 20 substrates were placed randomly in the simulation box with the box size l and periodic boundary conditions. Two association/decay reaction types were defined: $\mathrm{S} + \mathrm{E} \underset{k_-}{\overset{k_+}{\rightleftharpoons}} \mathrm{ES}$ and $\mathrm{P} + \mathrm{E} \xleftarrow{k_c} \mathrm{ES}$ with intrinsic reaction rates λ_+,λ_- and λ_c for complex formation, decay into substrate and enzyme and decay into product and enzyme, respectively. The reaction radius σ was set for both reaction types to be 1. A desired simulation length $M = 2^{14}$ and length of the time step $\Delta t = 0.05$ was set. $1/\kappa = \sqrt{\lambda_+/D}$ can be defined as the penetration length into the the reaction square. Reaction distance should be larger than the mean displacement traveled with one step. Otherwise the time of one particle staying within the reaction radius and thus the reaction rate would have large errors due to finite time step errors. In this simulation setup with $\sigma = 1$ and $\Delta t = 0.05$ and regardless of α the particles on average travel for $n = 20$ steps $\sqrt{6 K_\alpha n \Delta t^\alpha} \sigma$ to overcome the distance σ. Further the reaction probability as approximated in eq. (2.19) should be a lot smaller than $P(\Delta t) = \lambda \Delta t \ll 1$. Otherwise that approximations fails to describe the correct reaction probability $P(t) = 1 - \exp(-\lambda t)$. Simulations for various λ_+ ,λ_-,λ_c, box size l and α were performed. The results are discussed in the next two sections.

3.3 Results for Normal Diffusion

First simulations with normal diffusion were set up to have a connection to the results from the Smoluchowski and Erban-Chapman problem. The difference in kinetics of the Michaelis Menten mechanism to the Erban-Chapman problem is a possible blocking of the enzyme. Thus slowing down the reaction speed and a higher local concentration of the substrates in close proximity to the enzyme because of the back reaction. At first a reaction similar to the Erban-Chapman problem was aimed to simulate. Therefore $\lambda_- = 0$ was chosen to neglect the effect of a higher local concentration of substrates and $\lambda_+ > \lambda_c$ to neglect enzyme blocking. Thereafter the normal MM mechanism was studied.

3.3.1 Results for one Way Reactions

The first simulations was performed under normal diffusion $\alpha = 1$ and with $\lambda_- = 0$ in a simulation box of size $l^3 = 8^3$. The reaction mechanism results in:

$$\mathrm{S} + \mathrm{E} \xrightarrow{k_+} \mathrm{ES} \xrightarrow{k_c} \mathrm{P} + \mathrm{E} \tag{3.10}$$

$\lambda_+ = 0.1$ was set to be the rate limiting step in the reaction chain and $\lambda_c = 1.0$ was set to reproduce approximately the Erban-Chapman problem. The average normalized number of substrates $c_S(t)/c_{S_0}$, the normalized number of products $c_P(t)/c_{S_0}$ and the averaged number of complexes $c_{ES}(t)$ (over 2544 runs) were observed and visualized in a loglog plot in fig. 3.1. Every run had a new random (uniformly distributed) initial position of the substrate molecules. The simulated concentrations are shown as solid lines. The curves were fitted to obtain k_+ with the quasi-steady state approximation from eq. (3.4). The microscopic reaction rates and macroscopic reaction rate for a uni-molecular reaction should be similar $\lambda_c = k_c$. With all macroscopic rates available, the MM kinetics with the quasi-steady state approximation for the substrate were plotted from eqs. (3.4) to (3.7) as dashed lines in fig. 3.1. A blue bar in the plot indicates the time during which the radial distribution was observed. It was assumed that after 20 steps a stationary distribution was reached. The assumption was based on an approximated constant average number of complexes from there on. The radial distribution of the substrates around the enzyme/complex from 0 to the boundary of the simulation box $0 < r < 4.0$ was plotted in fig. 3.2. It was obtained by averaging over a normalized histogram of substrate particles. The Erban-Chapman solution eqs. (5.19) and (5.20) was plotted with dashed lines. The Erban-Chapman radial distribution is reproducing with good accuracy the observed radial distribution obtained by averaging over the histograms. For a better agreement substrate particles should be placed at the boundaries during the simulation

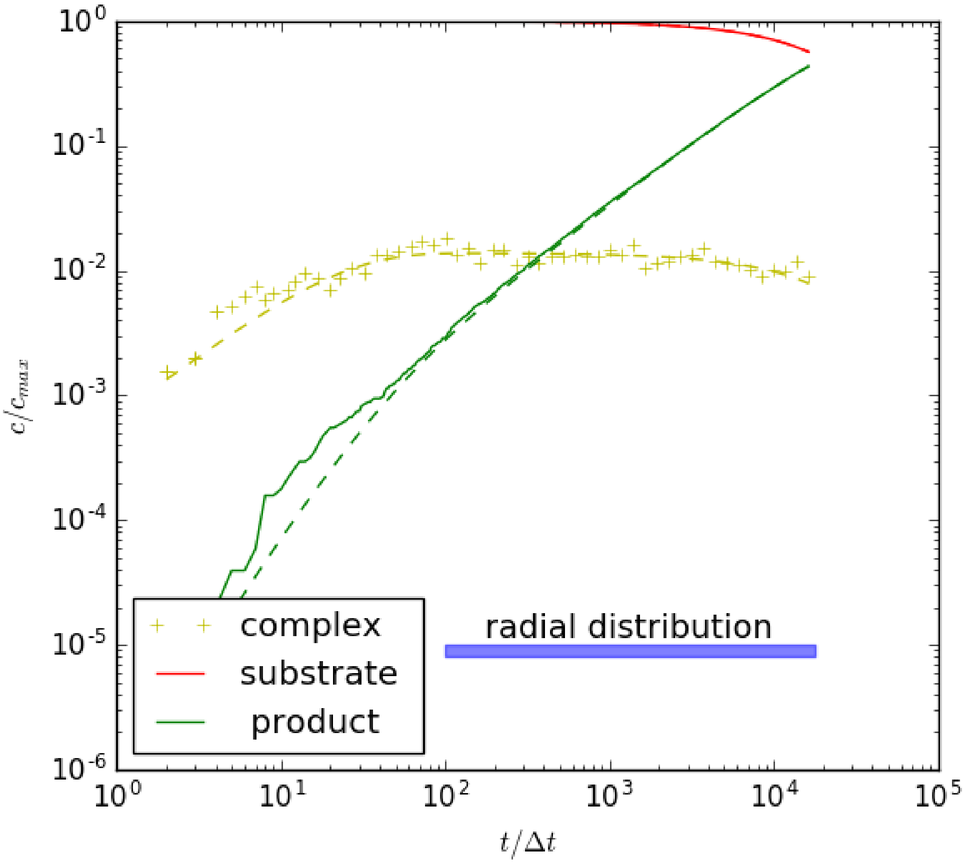

Figure 3.1: Normalized concentrations of substrate, product and complex and their fit with the quasi-steady state approximation for the substrate concentration are shown in the loglog plot. The blue bar in the plot indicates the area where the radial distribution was observed, which is plotted in fig. 3.2. Parameters were set to: $\lambda_+ = 0.1$, $\lambda_- = 0$, $\lambda_c = 1.0$ and the box size $l^3 = 8^3$.

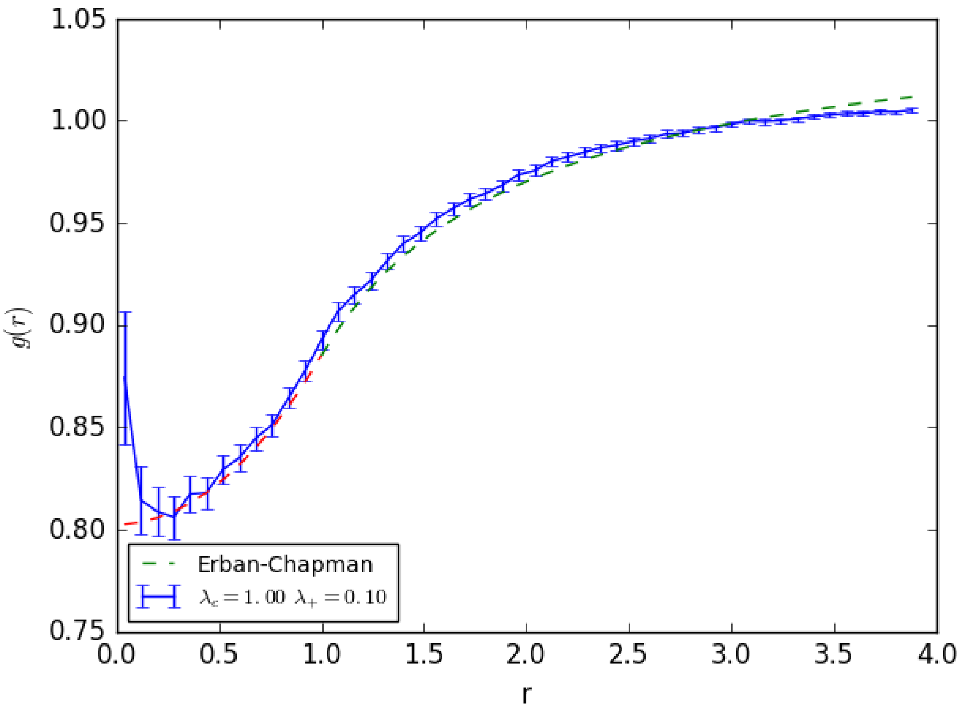

Figure 3.2: The radial distribution function of the substrates around the enzyme / complex was observed for $5 < t < 900$ and plotted as a blue line with an error-bar of the standard deviation. The Erban-Chapman result was plotted as a green dashed line for bigger than the reaction radius σ and a red dashed line for smaller than σ. Parameters were set to: $\lambda_+ = 0.1$, $\lambda_- = 0$, $\lambda_c = 1.0$ and the box size $l^3 = 8^3$.

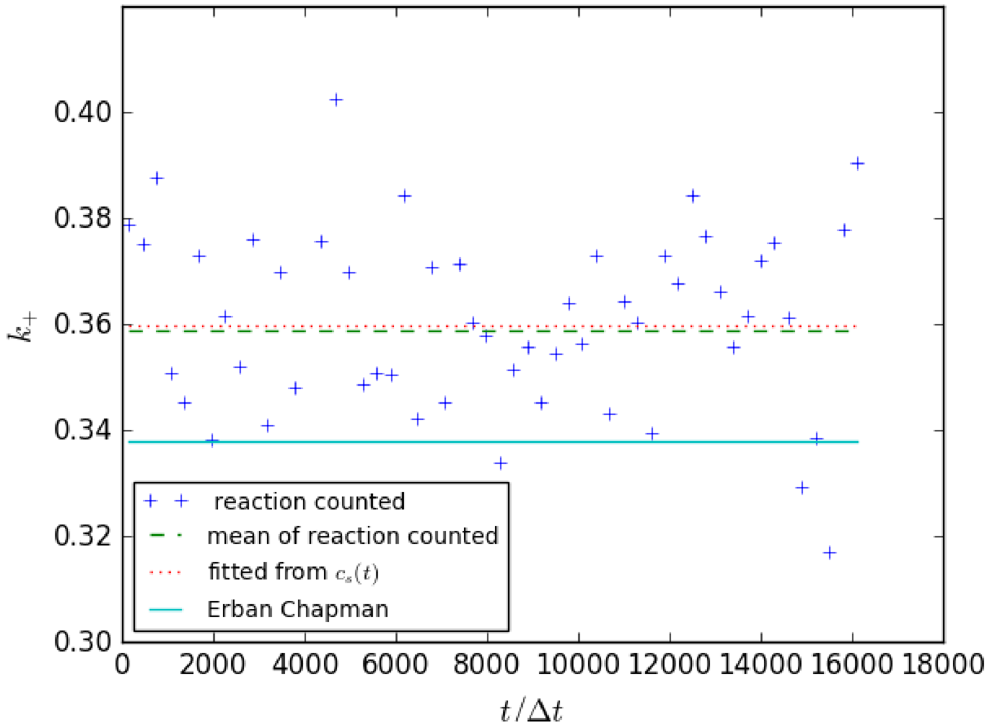

Figure 3.3: A comparison of k_+ from three different calculations. k_+ was calculated from the number of reactions with eq. (3.11) and marked as blue crosses. The Mean of this k_+ is plotted as a green dashed line. The result for k_+ from the fit of the substrate concentration eq. (3.4) with the QSSA is plotted as a red dotted line and the result form the Erban-Chapman eq. (2.16) problem is plotted as a solid cyan colored line. Parameters were set to: $\lambda_+ = 0.1$, $\lambda_- = 0$, $\lambda_+ = 1.0$ and the box size $l^3 = 8^3$.

to get a stationary concentration. The macroscopic reaction rate k_+ was calculated from the number of reactions $N_{reaction}$ of the reaction S + E $\xrightleftharpoons{k_+}$ ES. k_+ can be calculated from the reaction number change as:

$$k_+ = \frac{dN_{reaction}}{dt}\frac{1}{Vc_Sc_E} \tag{3.11}$$

V is the volume of the simulation box. Numerically the difference of the average reaction number was calculate. k_+ was very noise. It could be smoothed by averaging over 300 time steps. The result was plotted in fig. 3.3 as blue crosses. The average of these blue crosses was plotted as a dashed green line. The result for k_+ from the fit of the substrate concentration eq. (3.4) with the QSSA was plotted as a red dotted line and the result form the Erban-Chapman eq. (2.16) problem was plotted as a solid cyan colored line.

On the other hand a setup were reaction kinetics are limited by diffusion was tried to setup. Therefore $\lambda_c = 1.0$, $\lambda_- = 0$ and the box size $l^3 = 8^3$ were set fixed and $1 \leq \lambda_+ \leq 3.0$ scanned until diffusion becomes the rate limiting step. The macroscopic rates were obtained by fitting the substrate concentration with eq. (3.4). The fastest possible reaction should be limited by eq. (2.13) to be $k_+ = 2.094$. Even higher reaction rates were observed for $\lambda_+ = 2.0$ and 3.0 possibly because no extra particles were placed at the boundaries to indeed have a quasi stationary distribution. The radial distribution function was again obtained by a histogram observed for $5 < t < 900$ and compared with good agreement to the Erban-Chapman result in fig. 3.5. Even for the closest scenario to reactions being limited by diffusion the quasi steady state approximation still should hold because of $0.002 \approx c_{E_0} \ll K_M \approx 0.04$ as stated by [30].

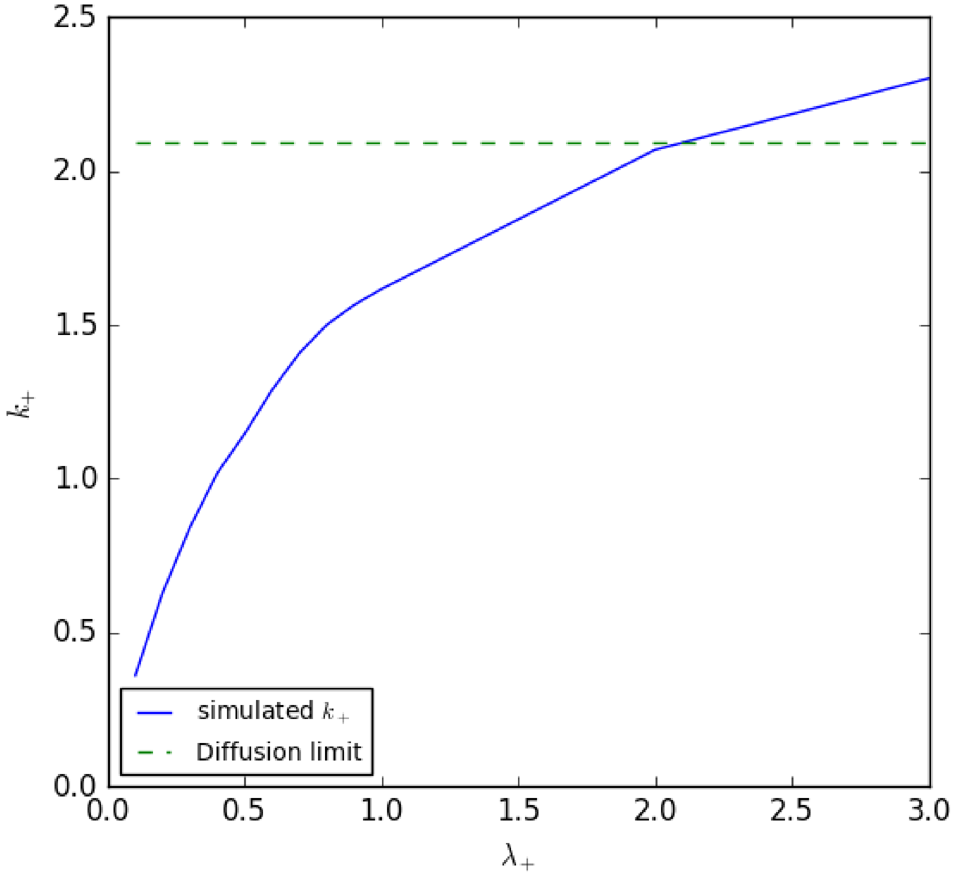

Figure 3.4: Parameters were set to: $\lambda_c = 1.0$, $\lambda_- = 0$ and the box size $l^3 = 8^3$. The blue solid line shows macroscopic rates k_+ in respect to microscopic rate $1 \leq \lambda_+ \leq 3.0$. The macroscopic rates are obtained with a fit of the substrate concentration eq. (3.4) with the QSSA. The diffusion limit eq. (2.13) is plotted as the dashed blue line.

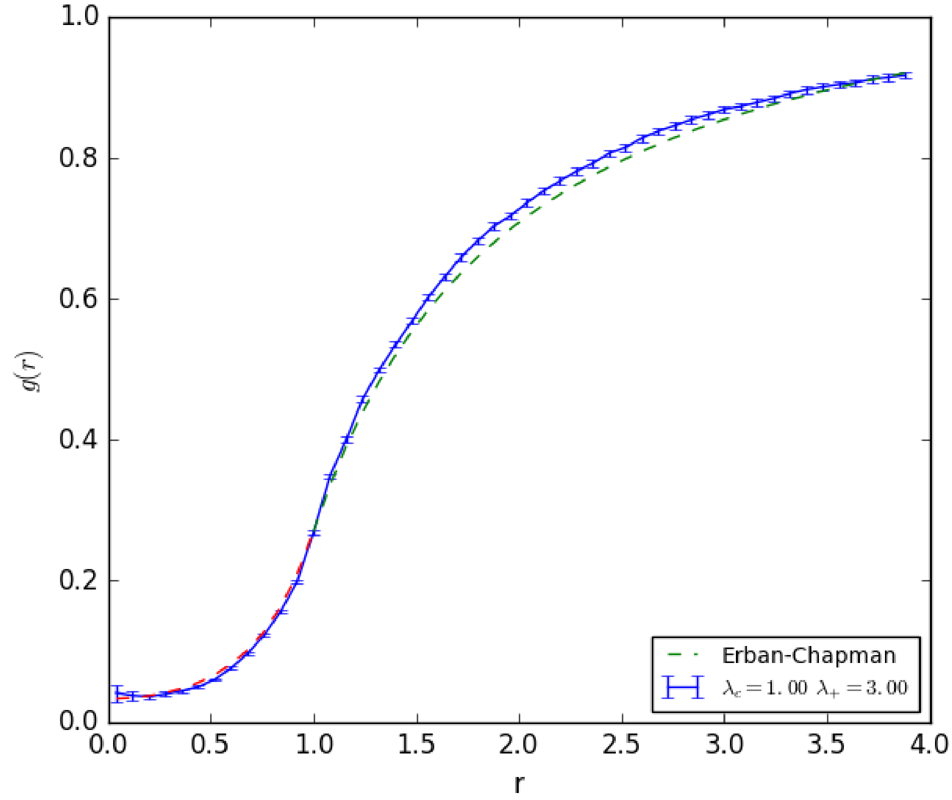

Figure 3.5: The radial distribution function of the substrates around the enzyme / complex was observed for $5 < t < 900$ and plotted as a blue line with an error-bar of the standard deviation. The Erban-Chapman result was plotted as a green dashed line for bigger than the reaction radius σ and a red dashed line for smaller than σ. Parameters were set to: $\lambda_+ = 3.0$, $\lambda_- = 0$, $\lambda_c = 3.0$ and the box size $l^3 = 8^3$.

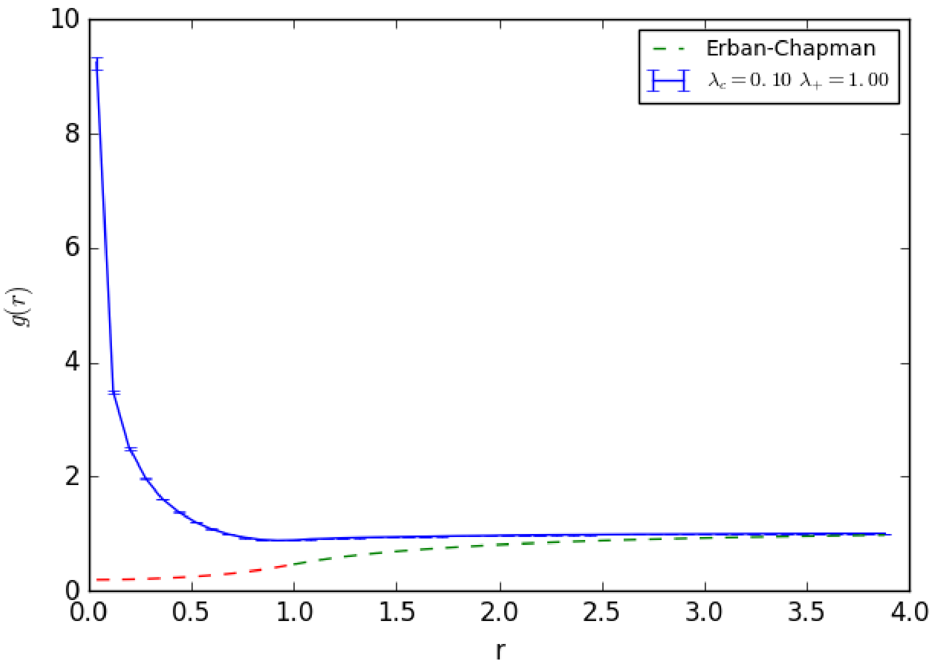

Figure 3.6: The radial distribution function of the substrates around the enzyme / complex was observed for $5 < t < 900$ and plotted as a blue line with an error-bar of the standard deviation. The Erban-Chapman result was plotted as a green dashed line for bigger than the reaction radius σ and a red dashed line for smaller than σ. Parameters were set to: $\lambda_+ = 1.0$, $\lambda_- = 1.0$, $\lambda_c = 0.1$ and the box size $l^3 = 8^3$.

3.3.2 Results for the MM mechanism

The first scenario of the MM mechanism was $\lambda_- > \lambda_c$ and $\lambda_+ > \lambda_c$ to have a local higher concentration of substrates around the enzyme. The radial distribution function was plotted in fig. 3.6 with the Erban-Chapman result as a reference. Determining $k_{+fit} = 4.34$ from the fit of eq. (3.4) results in a lot higher reaction rate than the Erban Chapman result $k_{+erban} = 1.25$. It is the result of the high local concentration of substrates around the enzyme. eq. (3.4) however, is based on the mass action law with homogeneously distributed substrates. The fits from the quasi steady state approximation with k_{+fit} and the average and not local concentration are still in well agreement with the data from the simulation. This can be seen in x-log plot in fig. 3.7. Also the method of counting reactions eq. (3.11) is based on an average concentration and results in similar macroscopic reaction rate $k_{+count} = 4.39$.

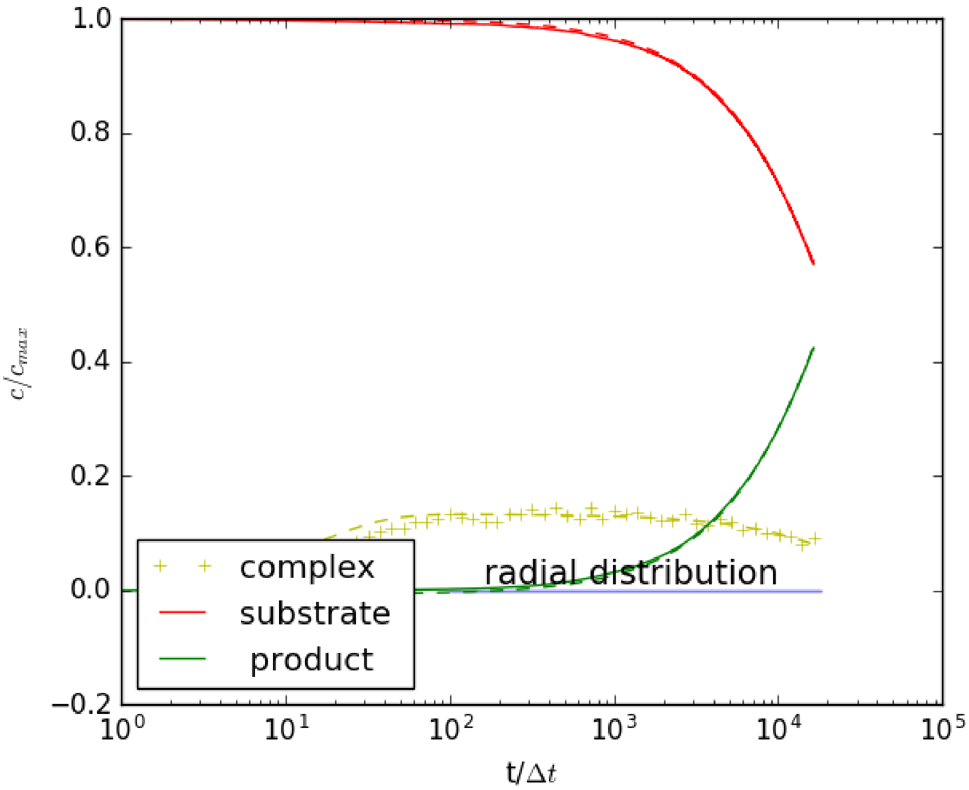

Figure 3.7: Normalized concentrations of substrate, product and complex and their fit with the quasi-steady state approximation for the substrate concentration are shown. The blue bar in the plot indicates the area where the radial distribution was observed, which is plotted in fig. 3.2. The remaining Parameters were set to: $\lambda_+ = 1$, $\lambda_- = 1$, $\lambda_c = 0.1$ and the box size $l^3 = 8^3$.

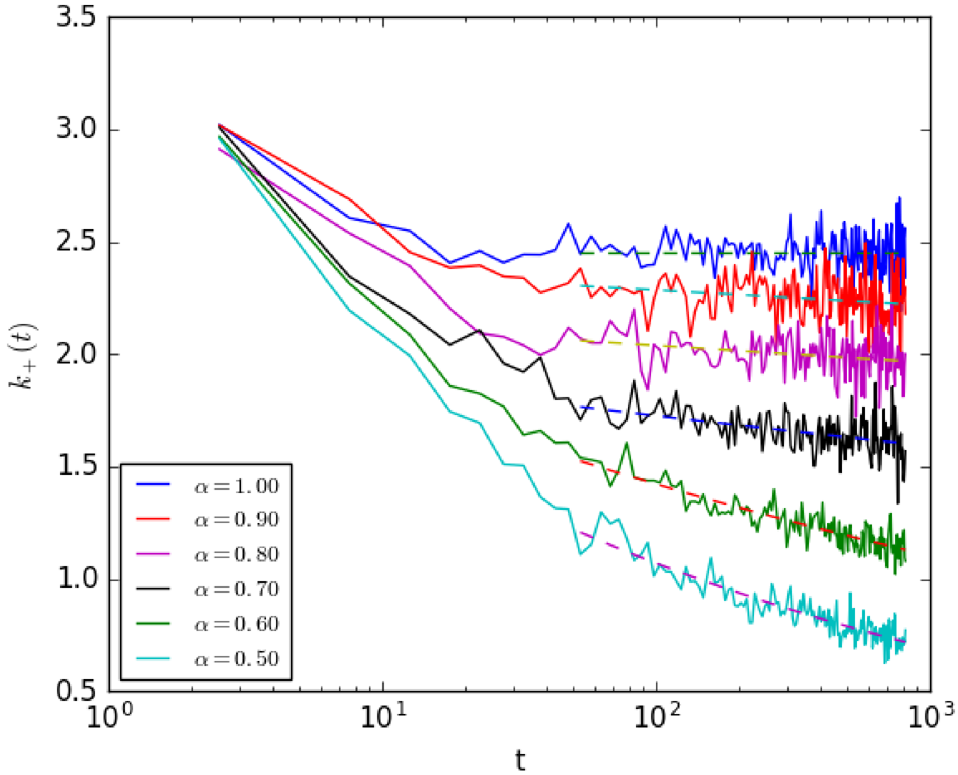

Figure 3.8: Form the number of reactions $k_{+count}(t)$ was calculated via eq. (3.11) and displayed as solid lines for $0.5 \leq \alpha \leq 1.0$. Witheq. (3.12) the fractal like kinetics exponent h was fitted and displayed as dashed lines in the plot. The remaining parameters were set to: $\lambda_+ = 1.0$, $\lambda_- = 1$, $\lambda_c = 1.0$ and the box size $l^3 = 8^3$.

3.4 Results for fBm

The mass action law does not hold anymore for reactions with fractional Brownian motion. Kopelman suggested for percolation cluster, in which particles diffuse anomalously, to have time depended macroscopic reaction rates for bi-molecular reaction of the form [33]:

$$k(t) = k_0 t^{-h} \qquad \text{for} \qquad 0 \leq h \leq 1 \qquad \text{and} \qquad t \geq 1 \tag{3.12}$$

to do: check how anomalous diffusion is related to fractal like kinetics factor h fig. 3.8. Can be shown that k(t) indeed describes the kinetics of MM with fractional Brownian motion.

3.5 Conclusion

The simulation model is capable of reproducing Smoluchwoskis and Erban-Chapman theoretical results for a Bi-molecular reaction. The simulation model can be described by Michaelis Menten kinetics for the quasi steady state approximation for normal diffusion but not for anomalous diffusion. Michaelis Menten reactions in a diffusion controlled regime with fractional Brownian motion are of fractal type. The modeling of biological reaction-diffusion dynamics with fBm can be interesting in a large system with a high number of particles not involved in the reaction mechanism but a small number of reactants, which diffuse anomalously. The large number of particles not have to be simulated explicitly. There influence on diffusion of the reactants is incorporated in fBm. The missing particle-particle interactions might get negligible with a low density of particles.

4 Summary

Cholesky, Davis Harte, our naive and Lowen algorithm for fractional Brownian motion have been implemented and analyzed in terms of accuracy and performance. Our implementation of Lowens algorithm turned out not to be exact as claimed by the author. Davis-Harte method turned out to be both exact and fast $\mathcal{O}(Mlog(M))$ with M the trajectory length. Davis-Harte and Lowen method was implemented in RevReaDDy. Besides the implementation of fBm many modifications to RevReaDDy were done to deal with our set of questions. A new reaction type and new observables were implemented. Some old observables were modified. A simulation setting with one enzyme and 20 randomly distributed substrates for the Michaelis Menten mechanism was set up and studied under normal Brownian motion and under fractional Brownian motion. Theoretical results from the Smoluchwoski problem of a diffusion controlled bi-molecular reaction and theoretical results for a bi-molecular reaction with microscopic reactions within close proximity to the enzyme could be reproduced by the simulation. It could be shown that the quasi steady-state assumption is indeed reproducing the kinetics of the Michaelis Menten mechanism for our setting, although this approach is not considering a non uniform spatial distribution.

For fractional Brownian motion with $\alpha < 1$ and $t < 1$ a general slowing down of reactions compared to normal diffusion was shown. Reaction rates are time depended for MM with fBm if reaction speed is controlled by diffusion, as Kopelman suggested for particles performing reactions in a percolation cluster ($k(t) = k_0 t^{-h}$). The kinetics are of fractal type.

As an outlook of the thesis a mathematical model for fractal Brownian motion and Michaelis menten mechanism for 3D could be developed. FBm with forces could be studied. Although a algorithm with possible potentials included will probably be very slow.

5 Appendix

5.1 From Central Limit Theorem to Gaussian Distribution

In the following the Central Limit Theorem will be applied to calculated the distribution of Y, $\rho(y)dy = P(y < Y < y + dy)$ in the limit of large N , with Y being defined as the sum of an random variable:

$$Y = \frac{1}{\sqrt{N}} \sum_{j=1}^{N} X_j \tag{5.1}$$

The Generating function for a random variable Y is:

$$G_Y(k) = \langle e^{ikY} \rangle = \int e^{ikY} \rho(y) dy \tag{5.2}$$

eq. (5.1) can be inserted into the generating function, which results in:

$$G_Y(k) = \langle e^{\frac{ik}{\sqrt{N}} \sum_{j=1}^{N} X_j} \rangle$$
$$G_Y(k) = \langle \prod_{j=i}^{N} e^{\frac{ik}{\sqrt{N}} X_j} \rangle$$

If all X_j are independent, then:

$$G_Y(k) = \prod_{j=i}^{N} \langle e^{\frac{ik}{\sqrt{N}} X_j} \rangle = e^{\sum_{j=1}^{N} A_j(\frac{k}{\sqrt{N}})} \tag{5.3}$$
$$\text{with } A_j(\frac{k}{\sqrt{N}}) = ln \langle e^{\frac{ik}{\sqrt{N}} X_j} \rangle$$

For large N behavior, we assume $\frac{k}{\sqrt{N}} << 1$ and expand

$$A_j(\frac{k}{\sqrt{N}}) = ln(1 + \langle X_j \rangle \frac{ik}{\sqrt{N}} - \langle X_j^2 \rangle \frac{k^2}{2N} + \mathcal{O}(N^{-\frac{3}{2}})) \tag{5.4}$$

with a finite variance $\sigma_i^2 = \langle X_i^2 \rangle$ and the mean $\langle X_i \rangle = 0$

$$A_j(\frac{k}{\sqrt{N}}) = -\sigma_j^2 \frac{k^2}{2N} + \mathcal{O}(N^{-\frac{3}{2}})) \tag{5.5}$$

Thus, the generating function for large N is:

$$G_Y(k) = e^{-\frac{\sigma^2 k^2}{2}} \tag{5.6}$$
$$\text{with } \sigma = \frac{1}{N}\sum_{j=1}^{N}\sigma_j^2$$

The distribution of Y can be calculated via the inverse Fourier Transform:

$$\rho(y) = \frac{1}{2\pi}\int_{-\infty}^{\infty} e^{-\frac{\sigma^2 k^2}{2}} e^{iky} dk \tag{5.7}$$
$$= \frac{1}{\sqrt{2\pi}\sigma} e^{-\frac{y^2}{2\sigma^2}} \tag{5.8}$$

$\rho(y)$ results in a Gaussian distribution.

5.2 From Gaussian Distribution to Gaussian Transition Probability

The conditional distribution function to be in x at time t if visited position y at time s can be written due to Bayes' theorem as a transition probability from y to x in time $t-s$ multiplied with the probability to be in y at time s:

$$\rho_{t,s}(x, y) = T_{t-s}(x|y)\rho_s(y) \tag{5.9}$$

Further due to particle conservation another relation holds:

$$\rho_t(x) = \int \rho_{t,s}(x, y)dy \tag{5.10}$$

Having an initial condition $\rho_s(x) = \delta(x - y)$:

$$\rho_{t,s}(x|y) = \int \rho_{t,s}(x, y)dy = \int T_{t-s}(x|y)\rho_s(y)dy \tag{5.11}$$
$$= \int T_{t-s}(x|y)\delta(x - y)dy = T_{t-s}(x|y) \tag{5.12}$$

5.3 Einstein Formula

The derivative of the mean variance of the Gaussian distribution in respect to time is defined as:

$$\frac{d}{dt}\delta\boldsymbol{r}^2(t) = \frac{d}{dt}\langle\Delta\boldsymbol{R}^2(t)\rangle = \frac{d}{dt}\int d\boldsymbol{r}\boldsymbol{r}^2 c(\boldsymbol{r}, t) = \int d\boldsymbol{r}\boldsymbol{r}^2\frac{\partial}{\partial t}c(\boldsymbol{r}, t) \tag{5.13}$$

Fick's second law can be applied:

$$= D \int_{-\infty}^{\infty} d\boldsymbol{r}\boldsymbol{r}^2 \Delta c(\boldsymbol{r}, t) \tag{5.14}$$

Assuming a reasonable assumption $c(\pm\infty, t) = 0$ and two times partial integration one can derive:

$$= -2D \int_{-\infty}^{\infty} d\boldsymbol{r}\boldsymbol{r} \nabla c(\boldsymbol{r}, t) \tag{5.15}$$

$$= 2Dd \int_{-\infty}^{\infty} d\boldsymbol{r} c(\boldsymbol{r}, t) = 2dD \tag{5.16}$$

For the initial condition $\boldsymbol{r}(0) = 0$, one gets the Einstein Formula: $\langle (\boldsymbol{r}(t) - \boldsymbol{r}(0))^2) \rangle = 2dDt$

5.4 Autocorrelation Function for fBm

Subsequently, the VACF in the frequency domain for Fractional Brownian motion can be calculated. The MSD is $\delta r^2(t) =< \Delta R(t) >= 2dK_\alpha t^\alpha$ with K_α being the generalized diffusion-coefficient:

$$\begin{aligned} \tilde{Z}(z) &= \int_0^\infty dt e^{izt} Z(t) \\ &= \frac{1}{2d} \int_0^\infty dt e^{izt} \left[\frac{d^2}{dt^2} \delta r^2(t) \right] \end{aligned}$$

Partial integration:

$$\overset{par.integ.}{=} \frac{1}{2d} \left(\underbrace{\left[e^{izt} \overbrace{\frac{d}{dt} 2dK_\alpha t^\alpha}^{=A(t)} \right]_0^\infty}_{\overset{\alpha \leq 2}{=} 0} - iz \int_0^\infty dt e^{izt} \left[\frac{d}{dt} \delta r^2(t) \right] \right)$$

$$A(t) = \frac{d}{dt} \overbrace{\left[\frac{2dK_\alpha t^{\alpha-1}}{\alpha} \right]}^{B(t)} = \frac{2dK_\alpha t^{\alpha-2}}{\alpha + (\alpha - 1)}$$

Partial integration and Tauber theorem:

$$\tilde{Z}(z) \overset{par.integ.}{=} -\frac{1}{2d}\left(\underbrace{\left[e^{izt}\overbrace{2dK_\alpha t^\alpha}^{=B(t)}\right]_0^\infty}_{\overset{\alpha\leq 1}{=}0} - (iz)^2\int_0^\infty dt e^{izt}\delta r^2(t)\right)$$

$$= -\frac{z^2}{2d}\int_0^\infty dt e^{izt}\delta r^2(t) \overset{\mathrm{Im}(z)>0}{=} K_\alpha\Gamma(1+\alpha)(iz)^{1-\alpha}$$

5.5 Erban-Chapman

The calculation can be started from eq. (2.7). This derivation can be found in [22]. The stationary distribution can be written as:

$$\left(\frac{\partial}{\partial_r}+\frac{2}{r}\right)D\frac{\partial\rho_t(r)}{\partial_r} = 0 \qquad \text{for} \qquad r \geq \sigma \tag{5.17}$$

$$\left(\frac{\partial}{\partial_r}+\frac{2}{r}\right)D\frac{\partial\rho_t(r)}{\partial_r} = \lambda_+\rho_t(r) \qquad \text{for} \qquad r \leq \sigma \tag{5.18}$$

For $r \leq \sigma$ a production term had been added to the continuity equation. The general solution can be written as:

$$\rho_t(r) = a_1 + \frac{a_2}{r} \qquad \text{for} \qquad r \geq \sigma \tag{5.19}$$

$$\rho_t(r) = \frac{a_3}{r}\exp\left[r\sqrt{\frac{\lambda_+}{D}}\right] + \frac{a_4}{r}\exp\left[-r\sqrt{\frac{\lambda_+}{D}}\right] \qquad \text{for} \qquad r \leq \sigma \tag{5.20}$$

with a_1, a_2, a_3, a_4 real constants. Just like in the calculation in diffusion limit the distribution at $r \to \infty$ is defined as the concentration of particle A $\rho_t(r \to \infty) = C_A$. Thus $a_1 = C_A$ and due to the continuity of the density distribution , $a_3 = -a_4$. Further, due to the continuity of the the flux $j_s(r)$ at $r = \sigma$ also a_2 and a_3 can be determined:

$$a_2 = C_A\left(\sqrt{\frac{D}{\lambda_+}}\tanh\left(\sigma\sqrt{\frac{\lambda_+}{D}}\right) - \sigma\right) \tag{5.21}$$

$$a_3 = \frac{C_A\sqrt{\frac{D}{\lambda_+}}}{2\cosh\left(\sigma\sqrt{\frac{\lambda_+}{D}}\right)} \tag{5.22}$$

The flux at $r = \sigma$ can be written as:

$$j^s(\sigma) = D\frac{\partial\rho_t(\sigma)}{\partial_\sigma} = -D\frac{a_2}{\sigma^2} \tag{5.23}$$

Gauss's theorem states that the negative flux of a quantity through a closed surface is equal to the production of that quantity inside the volume. Further The change of complex AB is proportional to the change of A inside the volume of of the sphere with $r = \sigma$. The total flux and thus the change of AB can be written as:

$$\frac{dC_{AB}}{dt} = -\int_{\partial V} j^s(\sigma)da = \int_{\partial V} D\frac{a_2}{\sigma^2}da = -4\pi D a_2 C_B \tag{5.24}$$

$$= 4\pi D C_B C_A \left(\sigma - \sqrt{\frac{D}{\lambda_+}}\tanh\left(\sigma\sqrt{\frac{\lambda_+}{D}}\right)\right) \tag{5.25}$$

5.6 Michaelis-Menten Kinetics

Michaelis-Menten kinetics are describing the following reaction: $\mathrm{S} + \mathrm{E} \underset{k_-}{\overset{k_+}{\rightleftarrows}} \mathrm{ES} \xrightarrow{k_c} \mathrm{P} + \mathrm{E}$. A set of differential equations can be formulated as a result of mass conservation and the mass action law:

$$\frac{dc_P(t)}{dt} = k_c c_{ES}(t) \tag{5.26}$$

$$\frac{dc_E(t)}{dt} = k_c c_{ES}(t) + k_- c_{ES}(t) - k_- C_E(t) C_S(t) \tag{5.27}$$

$$\frac{dc_S(t)}{dt} = k_- c_{ES}(t) - k_+ c_E(t) c_S(t) \tag{5.28}$$

$$\frac{dc_{ES}(t)}{dt} = -k_c c_{ES}(t) - k_- c_{ES}(t) + k_+ c_E(t) c_S(t) \tag{5.29}$$

With a quasi-steady-state approximation: $\frac{dc_{ES}(t)}{dt} = 0$ one can reduce labelquasisteadymichaelis to: $k_+ c_E(t) C_S(t) = k_- c_{ES} + k_c c_{ES}(t)$. A Rearrangement of this equation results in the Michaelis-Menten constant:

$$K_M = \frac{k_- + k_c}{k_+} = \frac{c_E(t) c_S(t)}{c_{ES}}. \tag{5.30}$$

From mass conservation law one gets: $c_E(t) = c_{E_0} - c_{ES}(t)$ After inserting this equation into the quasi-steady-state approximation of eq. (5.29), one gets:

$$c_{ES}(t) = \frac{c_{E_0} c_S(t)}{K_M + c_S(t)} \tag{5.31}$$

The combination of this eq. with the first differential eq. (5.27) defines the velocity of the reaction:

$$v(c_S(t)) = \frac{dc_P(t)}{dt} = k_c \frac{c_{E_0} c_S(t)}{K_M + c_S(t)} = v_{max} \frac{c_S(t)}{K_M + c_S(t)} \tag{5.32}$$

Bibliography

[1] A. P. Minton: *How can biochemical reactions within cells differ from those in test tubes?*, Journal of cell science **119**, 2863 (2006).

[2] F. Höfling and T. Franosch: *Anomalous transport in the crowded world of biological cells*, Reports on Progress in Physics **76**, 046602 (2013).

[3] B. B. Mandelbrot and J. W. Van Ness: *Fractional Brownian Motions, Fractional Noises and Applications*, SIAM Review **10**, 422 (1968).

[4] L. Michaelis and M. L. Menten: *Die kinetik der invertinwirkung*, Biochem. z **49**, 352 (1913).

[5] F. Höfling: *Stochastic processes and correlation functions*, University Lecture (2016).

[6] A. Fick: *On liquid diffusion*, Poggendorffs Annalen (1855).

[7] J. Fourier: *theorie analytique de la* (Firmin Didot, 1822).

[8] A. Einstein: *Über die von der molekularkinetischen theorie der wärme geforderte bewegung von in ruhenden flüssigkeiten suspendierten teilchen*, Annalen der Physik **322**, 549 (1905).

[9] M. von Smoluchowski: *Zur kinetischen theorie der brownschen molekularbewegung und der suspensionen*, Annalen der Physik **326**, 756 (1906).

[10] H. Qian: *Fractional brownian motion and fractional gaussian noise*, in *Processes with Long-Range Correlations* (Springer, 2003), pp. 22–33.

[11] D. Ton: *Simulation of fractional Brownian motion*, Master's thesis (2004).

[12] J. R. M. Hosking: *Modeling persistence in hydrological time series using fractional differencing*, Water Resources Research **20**, 1898 (1984).

[13] S. B. Lowen: *Efficent generation of fractional brownian motion for simulation of infrared focal-plane array calibration drift*, Methodology And Computing In Applied Probability **1**, 445 (1999).

[14] R. B. DAVIES and D. S. HARTE: *Tests for hurst effect*, Biometrika **74**, 95 (1987).

[15] P. F. Craigmile: *Simulating a class of stationary Gaussian processes using the Davies-Harte algorithm, with application to long memory processes*, Journal of Time Series Analysis **24**, 505 (2003).

[16] M. Timmer, J.;Koenig: *On generating power law noise*, Astronomy and Astrophysics **300**, 707 (1995).

[17] P. Horvai, T. Komorowski, and J. Wehr: *Finite time approach to equilibrium in a fractional brownian velocity field*, Journal of Statistical Physics **127**, 553 (2007).

[18] P. Waage and C. M. Gulberg: *Studies concerning affinity*, Journal of Chemical Education **63**, 1044 (1986).

[19] R. Erban, J. Chapman, and P. Maini: *A practical guide to stochastic simulations of reaction-diffusion processes* (2007).

[20] D. T. Gillespie: *Exact stochastic simulation of coupled chemical reactions*, The Journal of Physical Chemistry **81**, 2340 (1977).

[21] M. v. Smoluchowski: *Versuch einer mathematischen Theorie der Koagulationskinetik kolloider Lösungen* (????).

[22] R. Erban and S. J. Chapman: *Stochastic modelling of reaction–diffusion processes: algorithms for bimolecular reactions*, Physical Biology **6**, 046001 (2009).

[23] M. B. Flegg: *Smoluchowski reaction kinetics for reactions of any order* pp. 1–30 (????).

[24] J. Schöneberg and F. Noé: *Readdy - a software for particle-based reaction-diffusion dynamics in crowded cellular environments*, PLOS ONE **8**, 1 (2013).

[25] F. A. Abdullah: *Using fractional differential equations to model the michaelis-menten reaction in a 2-d region containing obstacles*, ScienceAsia **37**, 75 (2011).

[26] H. Berry: *Monte carlo simulations of enzyme reactions in two dimensions: fractal kinetics and spatial segregation.*, Biophysical journal **83**, 1891 (2002).

[27] S. Schnell and T. E. Turner: *Reaction kinetics in intracellular environments with macromolecular crowding: Simulations and rate laws*, Progress in Biophysics and Molecular Biology **85**, 235 (2004).

[28] T. E. Turner, S. Schnell, and K. Burrage: *Stochastic approaches for modelling in vivo reactions*, Computational Biology and Chemistry **28**, 165 (2004).

[29] J.-H. Jeon, A. V. Chechkin, and R. Metzler: *First passage behavior of multi-dimensional fractional brownian motion and application to reaction phenomena*, in *First-Passage Phenomena and Their Applications* (World Scientific Pub Co Pte Lt, 2014), pp. 175–202.

[30] B. O. Palsson: *On the dynamics of the irreversible michaelis-menten reaction mechanism*, Chemical Engineering Science **42**, 447 (1987).

[31] S. Schnell and C. Mendoza: *Closed form solution for time-dependent enzyme kinetics*, Journal of Theoretical Biology **187**, 207 (1997).

[32] S. Yuste and K. Lindenberg: *Subdiffusion-limited reactions*, Chemical Physics **284**, 169 (2002).

[33] R. Kopelman: *Fractal reaction kinetics*, Science **241**, 1620 (1988).